Synchrotron radiation applied to the study of heterogeneous model catalyst surfaces

2001 J. Phys.: Condens. Matter 13 11305

(http://iopscience.iop.org/0953-8984/13/49/313)

INSTITUTE OF PHYSICS PUBLISHING JOURNAL OF PHYSICS: CONDENSED MATTER

J. Phys.: Condens. Matter **13** (2001) 11305–11332 PII: S0953-8984(01)26670-3

Synchrotron radiation applied to the study of heterogeneous model catalyst surfaces

S Surnev, M G Ramsey and F P Netzer

Institut für Experimentalphysik, Karl-Franzens-Universität Graz, A-8010 Graz, Austria

Received 9 July 2001
Published 23 November 2001
Online at stacks.iop.org/JPhysCM/13/11305

Abstract

The application of synchrotron radiation-based experimental techniques for the characterization of model catalyst surfaces is reviewed. The planar model systems considered are distinguished by their heterogeneous surface character. Prototypical examples are discussed to illustrate various aspects of model catalyst surfaces and they include oxide thin films on metal single crystal substrates, metal nanoparticles deposited on ordered oxide films, thin layers of oxides on oxide substrates, heterogeneous bimetallic surfaces and metal single crystal surfaces decorated by oxide nanoparticles.

1. Introduction

Obtaining a molecular level understanding of catalytic reaction processes is still a fabulous challenge of the advanced catalytic sciences and a necessary prerequisite for the development of new high-technology catalysts, which aim for close to 100% selectivity for particular desired reaction products and high resistance to deactivation under severe process conditions. An array of modern ultrahigh vacuum (UHV) surface techniques is available at present, that allow surfaces to be precisely defined at the atomic level in terms of structure, composition, oxidation state and morphology. However, the practical industrial catalysts contain generally complex multicomponent systems, and such heterogeneity is detrimental to the application of these molecular-level techniques to their full potential. Efforts have been undertaken to integrate these UHV techniques into basic catalytic research, and the route which has been successfully employed involves the design of well-defined catalytic model systems, which incorporate some of the complexities of the real catalytic world but yet are tractable for the typical surface science probes. This surface science approach to heterogeneous catalysis is now well accepted and model catalyst behaviour can be used as standard for the evaluation of industrial catalyst systems [1–4]. A number of model systems have been used in the past 20–30 years, ranging from single crystal surfaces of metals to thin films of oxides, and many essential molecular ingredients of important catalytic reactions have been successfully identified. However, in order to narrow the gap in structural complexity and physico-chemical behaviour between the idealized surface science model systems and the real catalysts, the

heterogeneous character of most industrial catalysts has to be incorporated in some way into the more advanced model systems; this approach is referred to often as 'bridging the materials gap'. A comprehensive overview of catalytic model systems including classification and characterisation has been given recently in the review of Gunter *et al* [2].

In the present paper we will restrict our discussion to the so-called planar model catalyst surfaces, which are most suitable for the application of surface science and synchrotron radiation-based techniques because they involve structural order, in one way or the other, in most cases. The complications due to diffusion limitation into porous materials are absent on these surfaces and they can be prepared in UHV in a controlled way by *in situ* evaporation of one material onto well-ordered support surfaces of another material. We will not discuss single component model surfaces here, but rather in this paper the heterogeneity of the surfaces is the defining criterion for the catalyst model system character to be considered. Naturally, the results cited will concentrate on synchrotron radiation-based experiments, including UV and x-ray photoemission, x-ray absorption and x-ray microscopy techniques.

The paper is organised in the following way. In section 2 we describe the characterization of ordered oxide thin films on metal single crystal surfaces, which provide suitable starting materials for the construction of supported metal-particle catalysts, which in turn will be discussed in section 3. Section 4 investigates the properties of thin oxide layers formed on ordered surfaces of another oxide, thus imitating oxide-on-oxide catalyst surfaces. In section 5 some results from heterogeneous bimetallic surfaces will be presented, whereas in section 6 the concept of an 'inverse' model catalyst, i.e. metal single crystal surfaces decorated by oxide nanostructures, will be presented. It is not our intent to provide a comprehensive bibliographic review in this paper, but rather an illustration of the usefulness of methods utilizing synchrotron radiation for the characterisation of model catalyst surfaces and in so doing highlight some of the catalytically relevant issues.

2. Oxide films on metal single crystal substrates

The preparation of clean and well-ordered metal oxide surfaces from bulk oxide single crystals, used as catalysts or as supports for metal oxide catalysts, is not a trivial task. Also, the characterization of the electronic and geometrical structure of oxide surfaces or of adsorbates thereon by surface sensitive electron spectroscopy and imaging techniques is often hampered by charging problems due to their poor electronic conductivity. An alternative route, which has been successfully exploited in the past years, is to grow thin epitaxial films of oxides on metal substrates [5]. This technique eliminates the difficulties associated with the sample charging and allows the fabrication of high purity crystalline films with bulk-like-terminated surfaces.

Kuhlenbeck *et al* [6] have used this approach to investigate the electronic structure of thin NiO(100) films grown on a Ni(100) surface using angle-resolved photoemission (ARUPS) and near-edge x-ray absorption fine structure spectroscopy (NEXAFS). Figure 1 compares ARUPS spectra as a function of the photon energy for NiO(100)/Ni(100) (figure 1(a)) and for bulk NiO(100), cleaved in vacuum (figure 1(b)). The measured binding energies as a function of photon energies have been plotted as E versus $k_{[100]}$ dispersions in figure 2. In spite of the limited thickness, the band structure of the oxide films exhibits dispersions perpendicular to the surface compatible with bulk NiO(100). The larger peak widths in the NiO layers have been attributed by the authors to the presence of defects. The Ni 3d-derived bands at around 2 eV (figure 2) show no clearly observable dispersion, which has been explained with the high degree of localization of electrons on the Ni sites. At Γ the three O 2p levels are degenerate in the cubic environment of the NiO lattice. Along the Γ–X direction within the Brillouin

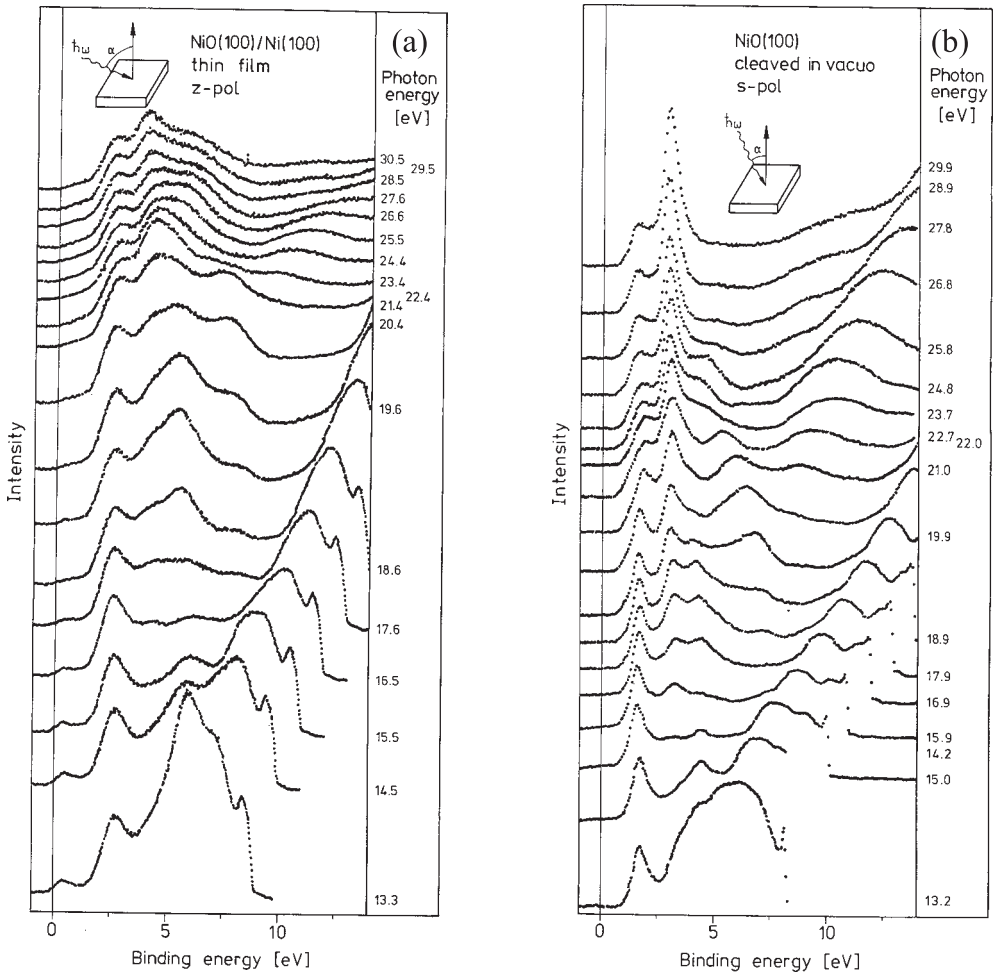

Figure 1. Series of normal-emission ARUPS valence band spectra: (a) NiO(100) film grown on Ni(100), photon angle of incidence $\alpha = 70°$; (b) cleaved NiO(100) single-crystal surface, $\alpha = 32.5°$. From [6] with permission.

zone the levels split into a non-degenerate O $2p_z$-derived band and a highly-lying (low binding energies) doubly degenerate O $2p_{x,y}$-derived band. The O $2p_z$ band has been identified by comparing the spectra taken with nearly s- and nearly p-polarized light. The authors have thus concluded that the electronic structure of the oxygen sublattice can be approximately described in a band structure picture [6]. The oxygen K-edge NEXAFS spectrum of the NiO(100) film (not shown) is almost identical to a corresponding spectrum of bulk NiO, demonstrating that not only the occupied electronic states, but also the unoccupied electronic states of the oxide film are comparable to those of bulk NiO.

Further in this paper [6], the results for the adsorption of NO on the NiO(100)/Ni(100) surface have been presented. NO chemisorbs weakly on the NiO surface with a desorption energy of ∼0.5 eV, as determined from thermal desorption spectroscopy (TDS) measurements. In order to obtain information on the orientation of the NO molecules with respect to the surface NEXAFS spectroscopy has been employed. Figure 3(a) shows N 1s NEXAFS spectra taken

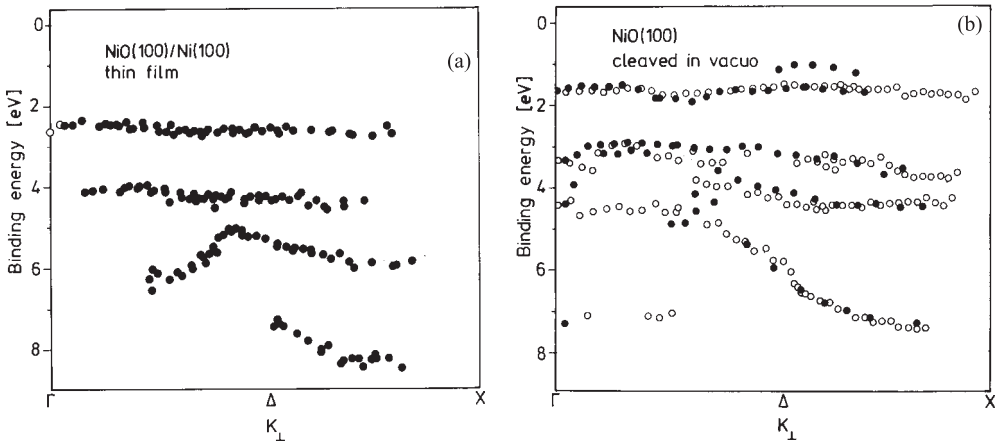

Figure 2. Experimentally determined valence band structure for (a) NiO(100)/Ni(100) and (b) *in vacuo* cleaved NiO(100). Solid circles represent data points in the first half of the second Brillouin zone, whereas open circles are data points folded back from the second half of the second Brillouin zone. From [6] with permission.

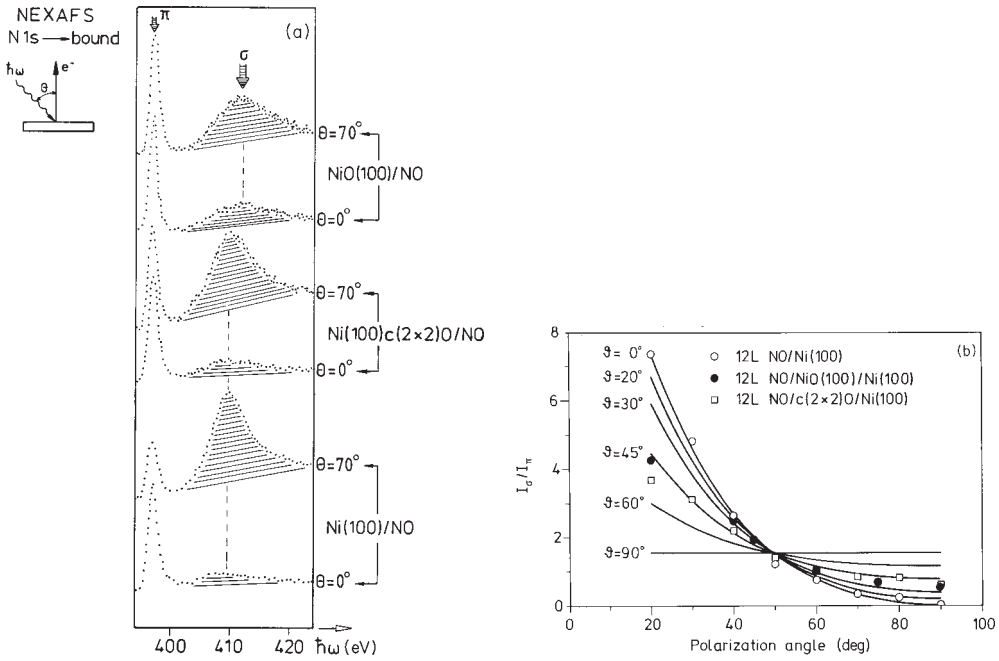

Figure 3. (a) N 1s NEXAFS results for NO adsorbed on NiO(100)/Ni(100) in comparison with the results for NO adsorbed on Ni(100) and c(2×2)O/Ni(100); (b) Experimentally determined σ/π intensity ratios as a function of the light incidence angle together with calculated curves for different molecular orientations of the adsorbed NO molecules. From [6] with permission.

at normal and at grazing incidence for NO adsorbed on NiO(100)/Ni(100), along with results for NO adsorbed on Ni(100) and c(2×2)O/Ni(100). The narrow peak at low photon energy

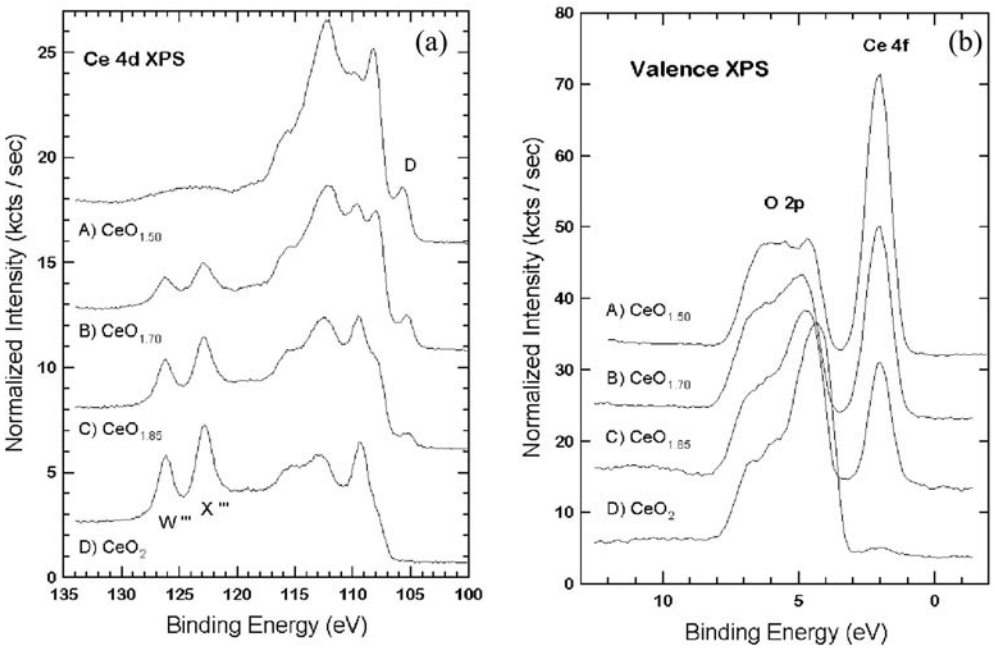

Figure 4. (a) Ce 4d core level and (b) valence band XPS spectra for ∼6 nm CeO_x grown on Ru(0001) with $1.5 < x < 2.0$. From [7] with permission.

is due to the N 1s-2π resonance and may be excited with the light polarization vector oriented perpendicular to the molecular axis. The broad band at higher photon energies is due to the so-called σ-shape resonance, which is polarized along the molecular axis. Therefore, by monitoring the variation of the relative intensities of σ and π resonances as a function of the light incidence angle, the angle between the molecular axis and the surface normal can be estimated. Figure 3(b) displays the experimental data together with calculated curves, according to a theoretical expression yielding the polar orientation of the molecular axis with respect to the surface normal. Based on this plot, Kuhlenbeck *et al* [6] concluded that NO molecules adsorbed on the NiO(100) surface are tilted by about 20° with respect to the surface normal. *Ab initio* cluster calculations [6] have shown that the tilting geometry of NO is driven by the stabilization of the lowest Ni 3d level.

The stoichiometry of CeO_2 (111) films grown on Ru(0001) surface has been characterised by soft x-ray photoelectron spectroscopy (SXPS) using synchrotron radiation in the paper of Mullins *et al* [7]. Figure 4 displays XPS spectra in the Ce 4d core level (a) and the valence band (VB) (b) regions for various oxide compositions. The latter was controlled by varying the oxygen pressure, at which the Ce metal has been deposited onto the Ru(0001) surface, from 1×10^{-7} Torr to 1×10^{-8} Torr. The W‴ and X‴ core-level peaks, which are absent in the $CeO_{1.5}$ spectrum, were used to estimate the proportion of Ce^{4+} in the sample, whereas the intensities of the D core level and the valence Ce 4f peaks were related to the amount of Ce^{3+}. The absence of a Fermi level in the valence spectra indicates that there is no metallic Ce present nor is the Ru substrate visible. It has been observed that the Ce 4d/O 1s intensity ratio does not correlate with the Ce(82)/O(510) Auger intensity ratio, the latter increasing with decreasing oxygen pressure. This has been attributed by Mullins *et al* to photoelectron diffraction effects [7].

Annealing reduced films to 500 K in an oxygen pressure of $\sim 10^{-7}$ Torr, followed by annealing at 1000 K, have been found to result in well-ordered and fully oxidized CeO_2 films, indistinguishable from those directly grown at higher oxygen pressure. Growing thick cerium oxides on Ru(0001) seems problematic, since the films appear to crack [7].

3. Metals deposited on oxide films

Nanometer-scale metal particles on well-ordered oxide surfaces constitute model systems which are closely related to industrial supported metal catalysts, since they contain both components and the realistic length scales of the heterogeneous system. The metal-on-oxide model systems may be prepared in a controlled way by UHV deposition of small quantities of metals on an epitaxially grown oxide thin film. The important aspects of these metal-on-oxide model systems are the following:

(i) the electronic structure of the metal particles as a function of particle size,
(ii) the geometry and size distribution of the metal particles,
(iii) metal-support interaction effects, and
(iv) the chemical reactivity of the composite surfaces. The latter may be gauged conveniently, in a first-order approach, by the adsorption of probe molecules.

Synchrotron radiation-based techniques can and have contributed significantly to these issues, and in this section we will illustrate the various aspects by presenting selected examples.

The ordered growth of metal clusters on oxide single crystal surfaces may be used to prepare metal phases in the form of microcrystallites with preferred orientation and structure. These small metal crystallites are well suited to determine the electronic state of the particles by probing the electronic energy bands of the metal clusters as a function of size via photoemission techniques. The appearance of valence band dispersions at a particular cluster size may be taken as an indication of the delocalization of the electronic system and thus of the transition of non-metallic to metallic state. Cai *et al* [8] have used this approach and investigated the size dependence of the electronic structure of Pd clusters deposited on an ordered Al_2O_3 film on Re(0001), using angle-resolved photoemission in conjunction with synchrotron radiation. Figure 5 shows normal emission photoelectron spectra of the valence bands of $Pd/Al_2O_3/Re(0001)$, taken at 30 eV photon energy, showing the evolution of the Pd 4d bands as a function of the Pd coverage. The spectral structures in the binding energy range 5–12 eV are the valence bands of the oxide substrate film, whereas the Pd 4d states occur at energies $\leqslant$4 eV. At low coverages the Pd 4d feature displays one single symmetric peak at $\sim$2 eV binding energy, but at higher coverages the width of the Pd structure increases and the peak maximum shifts to lower binding energy. For Pd coverages $\geqslant$1 monolayer equivalent (MLE), a second peak appears at the higher binding energy and intensity develops at the Fermi edge. After deposition of 30 MLE, the 4d valence band structure of metallic Pd with two peaks at 1.2 eV and 2.8 eV is fully developed. For Pd coverages $<$1 MLE the average cluster size is $<$20 Å and no density of states due to Pd is present at E_F; this is characteristic of a non-metallic state, and the absence of dispersion of the 4d feature with both the polar emission angle and the photon energy is consistent with non-metallic clusters, where the valence electrons are localized. In contrast, for coverages $\geqslant$1.5 MLE or an average cluster size of 30 Å and above there is notable density of states present at E_F and the 4d states display dispersion as a function of the emission angle and the photon energy (not shown here). This indicates the formation of energy bands due to delocalized electronic states. Based on these observations Cai *et al* have concluded that a non-metal to metal transition occurs at a Pd cluster size of $\sim$30 Å [8]. The

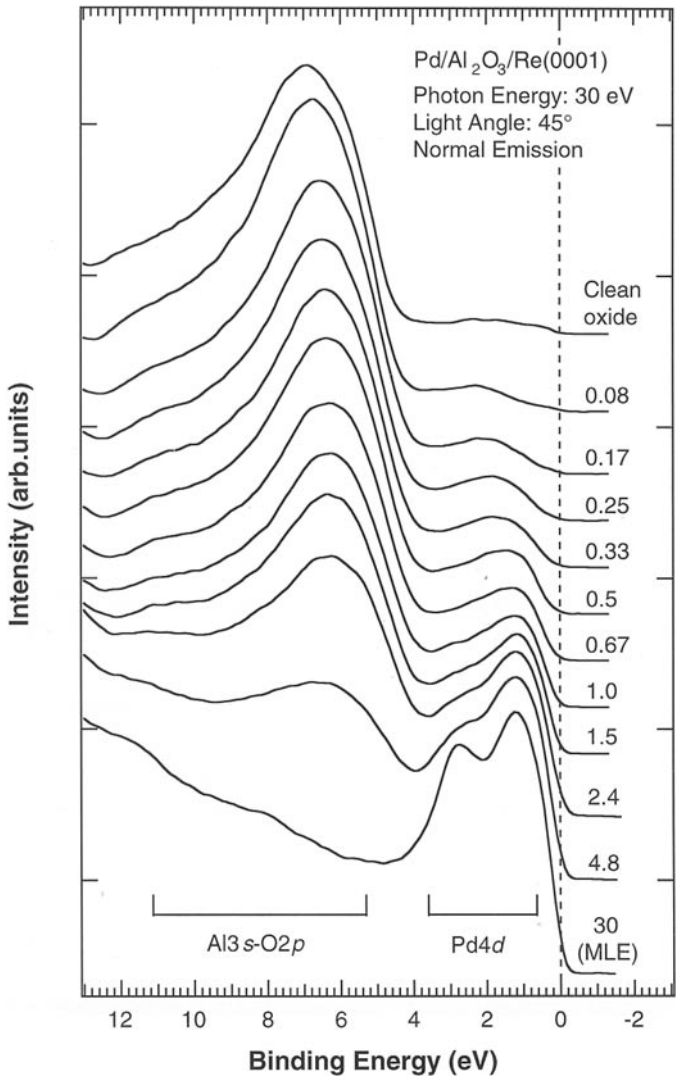

Figure 5. Normal emission valence band spectra of Pd clusters for coverages from 0.08 to 30 MLE. From [8] with permission.

quantitative observation of this size threshold of the formation of the metallic band structure in small supported clusters is interesting, but the answers to other questions such as what is the dependence of the extent of the dispersion on the cluster size, or what is the influence of the cluster-support interaction on the dispersion still await further experimental consideration.

The interactions of the metal component with the oxide support may be of decisive importance for the chemical reactivity behaviour of supported metal catalysts—cf for example, the so-called strong metal-support interaction (SMSI) effect [9]—but it also influences the physical parameters of the system, such as the growth behaviour and the morphology of the metallic phase. This is particularly significant for the more reactive metals at the left-hand side of the Periodic Table, where the metal atoms at the metal–oxide interface may become oxidised. As an example we mention here the work of Biener *et al* [10], who have

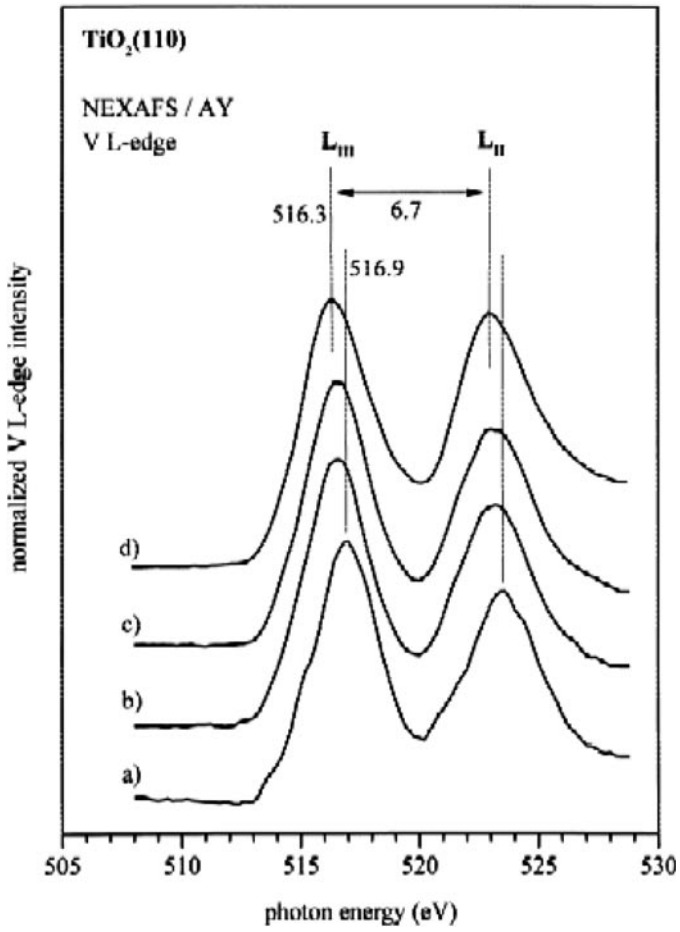

Figure 6. Normalized Auger-yield NEXAFS spectra of V-covered TiO_2 (110) in the V L-edge region: (a) 25s, (b) 40s, (c) 80s, (d) 600s. The deposition time is proportional to the V surface coverage (deposition rate $\sim$0.01 ML s^{-1}). From [10] with permission.

studied the growth and the electronic structure of vanadium on a TiO_2(110) surface. These authors have used semiconducting TiO_2 single crystal substrate samples, onto which vanadium was evaporated. On poorly conducting samples the XPS technique is sometimes difficult to apply for the determination of the chemical state of surface atoms because of surface charging effects. Conversely, the NEXAFS technique is well suited to study insulating samples because the excitation of a core electron into an unoccupied valence state involves a neutral final state. The technique thus probes the empty valence states projected onto the site with the core hole [11]. Both line shape and transition energy at the absorption edge can be used as a fingerprint to determine the chemical state and the local symmetry of the absorbing atom [12]. Figure 6 displays a set of NEXAFS spectra of the V L-edge (2p) region, which were recorded as a function of the V coverage on TiO_2 (110). The spectra contain two major features due to the absorption at the V L_{III} ($2p_{3/2}$) and L_{II} ($2p_{1/2}$) edges. The line shape of the V L-edge is determined by the relative magnitude of the electron–electron interaction versus the bandwidth, i.e. the presence or absence of multiplet splitting and by crystal field effects. At low coverages (spectrum a), the V L-edge peaks show fine structure wiggles indicating

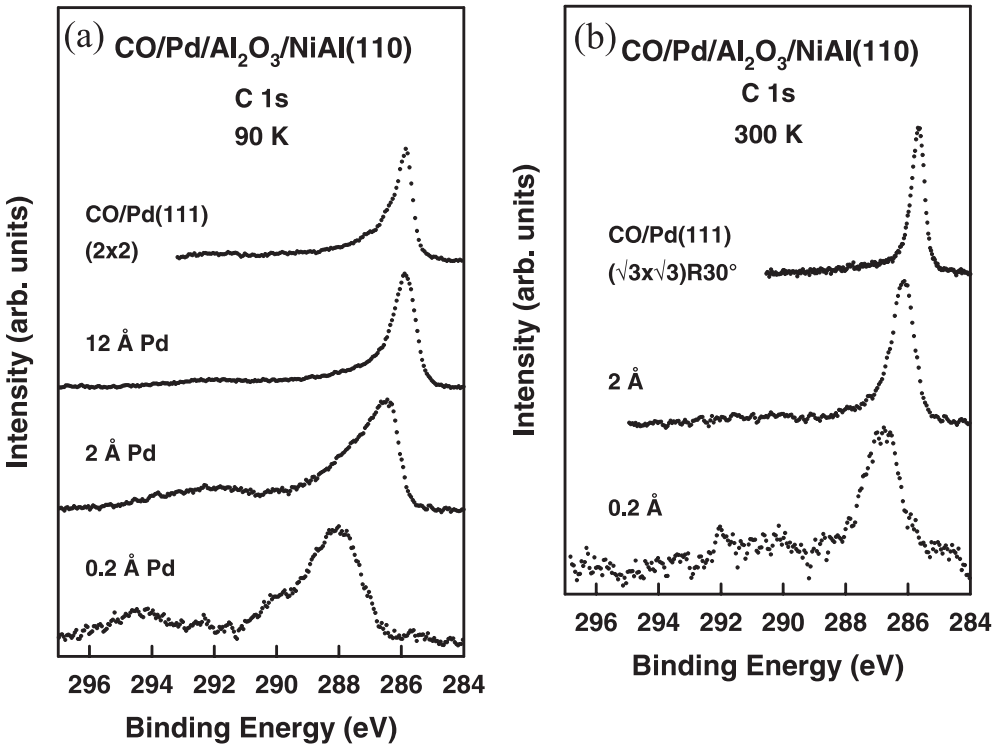

Figure 7. (a) C 1s spectra for CO adsorbed on Pd clusters of increasing size compared to CO/Pd(111)2 × 2. (b) C 1s spectra for CO adsorbed on two different cluster sizes after heating to 300 K compared to CO/Pd(111) ($\sqrt{3} \times \sqrt{3}$)R30°. From [10] with permission.

multiplet and/or crystal field splitting effects. This, together with the energetic peak positions (516.9 eV for the L_{III} structure), indicates that the V atoms at the interface are oxidized. Based on a correlation between the transition energy at the V L-edge and the oxidation state as established by Chen [12], Biener *et al* proposed the formation of V^{2+} cations at the TiO_2 interface [10]. With increasing V coverages the V L-edge shifts to lower photon energy, and after the deposition of V multilayers the L_{III} peak is observed at 516.3 eV (spectrum d). The fine structure of the feature is also lost at this stage, indicating a more metallic behaviour. The transition energy is not quite as low as expected for metallic vanadium, but a superposition of metallic vanadium atoms and V^{2+} cations might explain the results. The deposition of vanadium on TiO_2 in the submonolayer range thus leads to the formation of oxidized V atoms at the interface and a concomitant island growth morphology as revealed by separate STM measurements [10]. At multilayer coverages a more metallic vanadium film is formed, which however is granular and shows no long range order.

The study of the adsorption of probe molecules on metal–oxide model catalysts is a convenient approach to gauge the chemical reactivity of these systems; in addition, it often also allows to obtain complementary information on the physical parameters of these heterogeneous surfaces. Freund and collaborators have exploited the catalyst model character of systems based on epitaxial Al_2O_3 layers grown on NiAl(110) alloy surfaces, which they have decorated with metal particles. Here we cite some results of chemisorption experiments, which were obtained with the use of synchrotron radiation. Figure 7 describes the adsorption of CO

on Pd particles of different sizes, which were deposited onto Al_2O_3/NiAl(110). Figure 7(a) is a series of C 1s core level spectra after adsorption of CO at 90 K on ∼5 Å (0.2 Å Pd deposition), 20 Å (2 Å deposition), and 70 Å (12 Å deposition) mean diameter Pd particles [13]. For comparison, the spectrum of a CO (2×2) overlayer on Pd(111) ($\theta = 0.75$) is included in figure 7(a). Figure 7(b) shows the C 1s spectra taken after heating the CO-covered surfaces from 90 K to 300 K, after desorption of some weakly bound CO [13]. The C 1s peaks of figure 7(a) display a shift to lower binding energy with increasing particle size, an increasing line width and increasing asymmetric line broadening with decreasing particle size, and a pronounced shake-up intensity (at ∼6 eV higher BE) for the spectra from the smaller particles. The shift to lower binding energy with increasing particle size is typical and may be accounted for by a final state Coulomb effect [14]. Since the adsorption of CO in different surface sites may lead to C 1s BE shifts of 0.5–1 eV [15, 16], the stronger asymmetry at smaller particles sizes is interpreted by a multitude of adsorption sites on the smaller Pd particles. Note that even on the Pd(111) (2×2)-CO surface this asymmetry is apparent (top spectrum of figure 7(a)) and is caused by the two different CO adsorption sites (on-top and three-fold hollow) in this structure, which are more clearly resolved in the more recent core level spectra at very high resolution [17]. The behaviour in the shake-up region may be associated with the CO-metal coupling strength. Since stronger shake-up satellites are commonly found for more weakly bonded adsorbates [18], the increasing shake-up intensity indicates a decreasing CO-Pd interaction strength with decreasing particle size, i.e. more weakly bonded CO molecules on smaller Pd clusters; this is corroborated by CO thermal desorption spectra [14].

The C 1s spectra recorded after heating to 300 K (figure 7(b)) confirm the given interpretations: the peaks become more symmetric and sharper and the shake-up region loses intensity. The top spectrum of figure 7(b) is from a well-ordered Pd(111)$(\sqrt{3} \times \sqrt{3})$R30°-CO overlayer which contains only one single type of CO adsorption sites (three-fold coordinated hollow sites) [17] and thus displays a narrow C 1s peak shape. The spectral changes observed in the adsorbate spectra from 5 Å and 20 Å Pd particle sizes are consistent with the removal of weakly bonded CO in the heating step and suggest that the highly-coordinated CO species remain on the Pd particle surface.

Complementary information on the CO-Pd interaction has been derived from x-ray absorption spectroscopy (XAS) results, which are reproduced in figure 8 [19]. Figure 8 contains XAS spectra of transitions from the C 1s and O 1s core levels to the antibonding $2\pi^*$ orbital of CO adsorbed on the Pd clusters at 90 K, for the same cluster sizes as in figure 7. The data of figure 8 show that with increasing cluster size the widths of the absorption peaks increase. Since the width of this π resonance is thought to reflect the adsorbate–substrate hybridization strength between the CO $2\pi^*$ orbital and the metal states, the presented results indicate that the CO $2\pi^*$- Pd 4d hybridization increases with island size, thus confirming the increasing adsorption strength on the larger metal particles. From the energy positions of the XPS peaks (figure 8, lines below the C 1s XAS curves) relative to the XAS structures information on the electronic screening ability of the CO-Pd complex has been obtained. Sandell *et al* [19] concluded that the particle sizes >15 Å (>2 Å Pd deposition) behave metallic-like as a Pd bulk metal surface, whereas the 5 Å islands (0.2 Å Pd deposition) display a more reduced screening ability and CO adsorbed on these small clusters behaves similar to carbonyl complexes on an oxide support.

On alumina-supported Rh particle systems Frank *et al* [20] have investigated the probabilities for thermally induced dissociation of adsorbed CO as a function of particle size. The series of C 1s XPS spectra of CO adsorbed on large Rh particles (average size 10 000 atoms, 16 Å Rh deposition) as a function of heating to the indicated temperatures in figure 9 illustrates the potential of core level spectroscopy with synchrotron radiation to

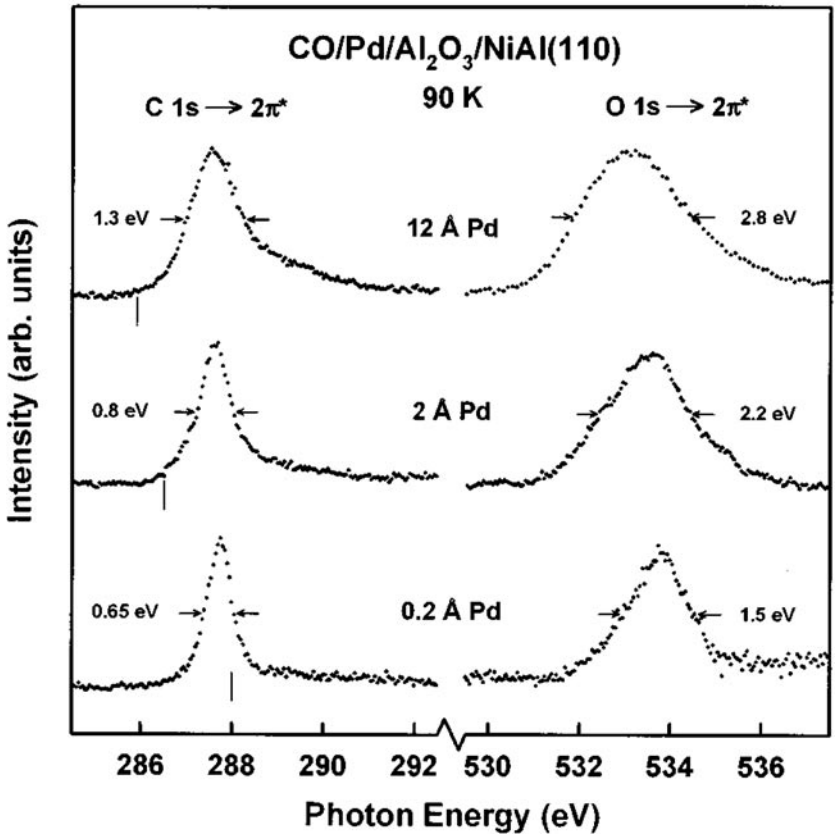

Figure 8. X-ray absorption spectra for CO adsorbed on Pd clusters of increasing size. The lines below the C 1s XAS spectra represent XPS binding energies. From [19] with permission.

follow the dissociation of adsorbed species. The signal at 285.8 eV is typical for molecularly adsorbed CO, whereas the feature appearing at the lower BE of ∼284 eV after heating to temperatures $\geqslant$350 K is fully compatible with atomic carbon in its carbidic form. This feature is due to CO dissociation. The quantitative evaluation of the C 1s signal intensities gives the ratio of molecular to dissociated CO for various temperatures and similar results may be obtained for various particle sizes. For small particles the dissociation activity has been found to increase with particle size until a broad maximum is reached for particles containing an average of 100–200 atoms [21]. For larger particles the fraction of dissociated CO decreases to values approaching those observed on stepped Rh single crystal surfaces. The authors have argued that a particular range of particle sizes may stabilize a high density of low-coordinated surface atoms at steps, kinks and other defect sites, which in turn lead to high dissociation activity [20].

The identification of reaction intermediates at surfaces is an important and necessary element in the elucidation of a catalytic reaction mechanism. A step in this direction is the work of Mullins [22, 23], who studied reactions on model emission control catalysts by soft x-ray photoemission, in particular the reaction of NO and CO on Rh/CeO_x. The catalysts were prepared by evaporating small amounts of Rh onto thin films of ceria, and the catalyst surfaces were characterised by core level and valence band photoemission spectra. C 1s

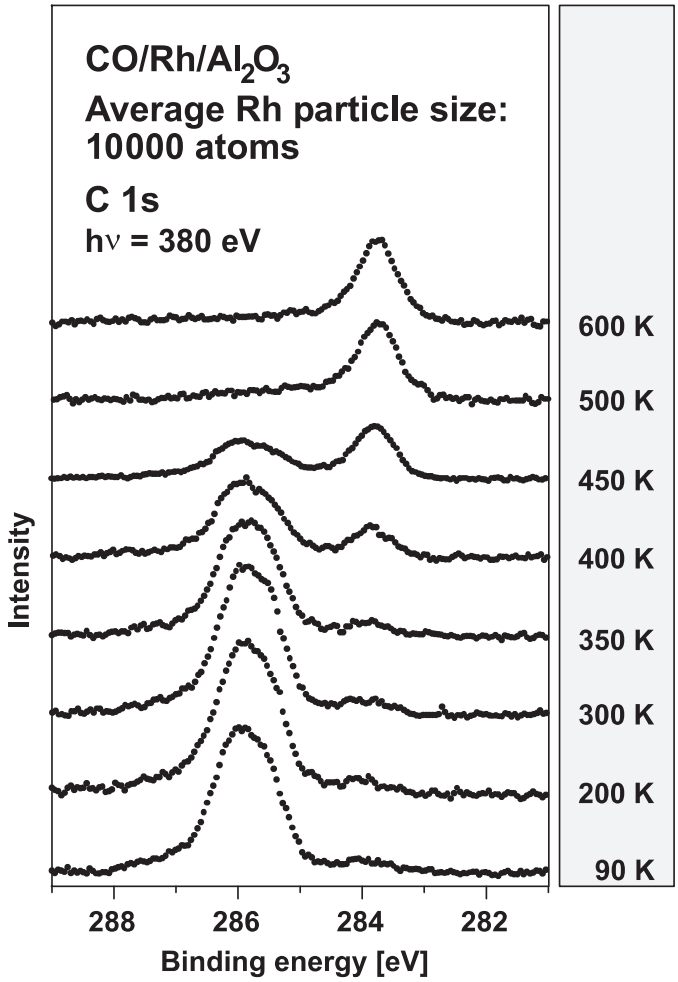

Figure 9. C 1s spectra taken after deposition of 16 Å Rh at room temperature, dosage of 40 L CO at 90 K and subsequent heating to the indicated temperatures. From [20] with permission.

and N 1s spectra following the coadsorption of NO and CO at 200 K on Rh deposited on reduced CeO_x and the evolution of the NO + CO covered surface with temperature are shown in figure 10. At 200 K, CO and NO adsorb molecularly on the Rh, but NO also dissociates partially; in addition, NO also forms NO^- and N^{3-} on the ceria [24]. On heating, a complex series of surface species as a result of dissociation followed by association is observed, which are characterised by their different C 1s and N 1s features. The evolving surface species have been identified by comparison with the spectra from the individual adsorbates and from related adsorbed molecules. The new surface species, which appear as a results of the NO–CO interaction at the catalyst for $T > 400$ K, comprise OCN and various CN type fragments, which eventually decompose into N_2 and CO at $T > 700$ K, the latter through a reaction of C with the CeO_x support material. The example of figure 10 demonstrates nicely the usefulness of XPS with its ability to distinguish between chemical species in more complex reaction sequences, even if the assignment of some of the intermediate species remains somewhat speculative at the present time.

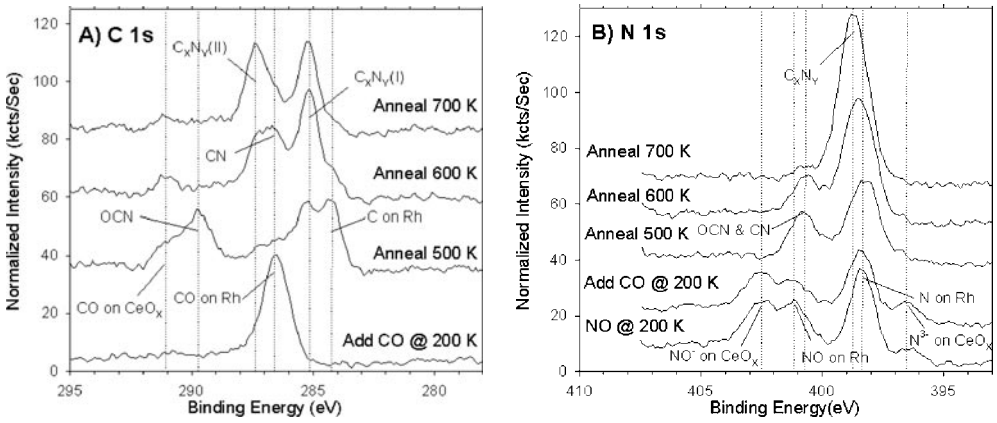

Figure 10. XPS spectra from NO and CO on Rh/CeO_x. (a) C 1s spectra excited by 405 eV radiation. (b) N 1s spectra excited by 515 eV radiation. A subsaturation coverage of NO was adsorbed at 200 K and CO was then added at 200 K. The sample was subsequently annealed as indicated. From [22] with permission.

4. Thin oxides on oxide substrates

Thin metal oxide films supported by a different metal oxide constitute a technologically important class of industrial catalysts. Despite this importance there is extremely little fundamental understanding of how the catalytic properties of such oxide-on-oxide systems are derived. This is presumably in part due to the fact that even model systems are reasonably complex and oxides present difficulties to a range of surface science techniques. The present goal is to understand the possible differences in the nature of the thin film to bulk oxides, i.e. their stoichiometry and structure. Also the growth mechanism of the thin film oxide is an intriguing scientific problem.

Recently, due to the technological interest in titania-supported vanadia catalysts, model studies of vanadium oxide films grown on $TiO_2(110)$ have been undertaken. Because of the possibility of vanadium existing in a number of different oxidation states, the focus of these studies has been on the vanadium oxidation state and the role of the oxide substrate.

For low coverages vanadium is partially oxidized by the TiO_2. With post oxidation (423 K for 2 min in 2×10^{-6} O_2) it has been claimed that ordered (1×1) VO_2 thin films up to 5 ML can be created. This has been supported by studies of the valence band with synchrotron radiation. In constant initial state (CIS) spectra the V 3d emission intensity around the 3p-3d threshold is similar to bulk VO_2. Differences in the O 2p CIS in both energy and intensity to those obtained from bulk VO_2 were suggested to arise from the bidimensionality of the 2 ML film investigated [25]. The band structure effects observed from the valence band spectra in normal emission as a function of photon energy were also claimed to be similar to bulk VO_2.

For 1 ML oxidized films two distinct vanadium oxide species are observed in the V 3p spectra at 39.8 eV (I) and 41.9 eV (II) which have been attributed to VO_2 and V_2O_5, respectively [26] (figure 11(a)). These two features display extremely different photoelectron diffraction behaviour as illustrated in figure 11(b). The V_2O_5 emission shows essentially no intensity variation with photon energy (figure 11(b); spectrum g) indicative of short range disorder. In contrast the VO_2 3p emissions intensity behaviour (figure 11(b); spectrum b) is similar to that of the Ti 3p, particularly in the less bulk sensitive low kinetic energy region. This suggests that the local structural environment of these V ions are very similar to the surface Ti ions thus indicating a rutile-type epitaxial growth. Single scattering spherical wave (SSC-SW)

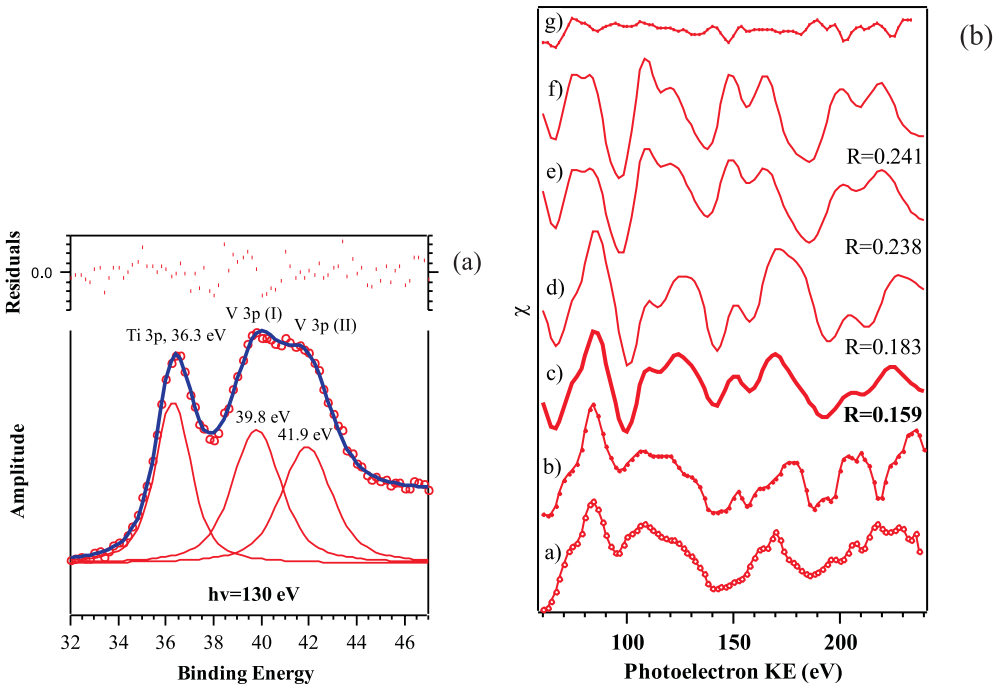

Figure 11. (a) Ti 3p and V 3p photoemission core levels from 1 ML vanadium stepwise deposited and post-oxidised on TiO_2. The Voigt fits for VO_2 (I) and V_2O_5 (II) are used in measurement of photoelectron diffraction behaviour. (b) Experimental photoelectron diffraction functions: the Ti 3p of the substrate (curve a), the V 3p (I) (curve b) and the V 3p (II) of the overlayer oxide (curve g). Single-scattering cluster spherical wave simulations for relaxed-mixed oxide bilayer (curve c), the relaxed VO_2 ML (curve d), the bulk-terminated mixed oxide bilayer (curve e), and bulk-terminated VO_2 (curve f). The *R* factors with respect to the V 3p (I) behaviour (curve b) are indicated. From [26] with permission.

simulations indicate that the monolayer is an intermixed VO_2/TiO_2 double layer where the vanadium atoms occupy the six-fold oxygen coordinated sites (figure 11(b); spectrum c).

Simultaneously, Madix and coworkers [27] have also been addressing the VO_x/TiO_2 system. They have been applying the naturally complementary combination of photoemission and photoabsorption spectroscopy with synchrotron radiation. For submonolayer deposition of vanadium metal on $TiO_2(110)$ the titanium at the interface is reduced from Ti^{4+} to Ti^{3+}. This is evidenced in the Ti 2p XPS by the appearance of a low binding energy shoulder and by the sharp t_{2g} and e_g related features in the Ti L edge NEXAFS becoming unresolved as the rutile structure's octahedral environment is replaced by a range of local symmetries (similar spectra to reduction by sputtering). Concomitantly, the V 2p emission indicates a single oxidized species with a $2p_{3/2}$ binding energy of 515.6 eV, i.e. 3.8 eV higher than the metal emission that appears at high V exposures. Although, given the scatter of reported values for powder oxides, this could be assigned to VO_2 or V_2O_3 the authors propose that it is due to V^{3+} (V_2O_3) [27].

In an attempt to produce a vanadium oxide film with a higher oxidation state (VO_2 or V_2O_5, thought to be important to catalytic activity) post-oxidation experiments with relatively high oxygen exposures (5×10^{-5} Torr O_2 for up to 20 min) at a variety of temperatures were made. For higher V exposures, where metallic V was evident, the post-oxidation resulted in characteristics of V_2O_3 species and no higher oxidation states where observed in XPS. Likewise the V 2p edge NEXAFS gave no evidence for a different oxidation state and the

comparison with XAS of V_2O_5 powder clearly rules out the presence of V_2O_5 [27]. Moreover, comparison with the single crystal vanadium oxide NEXAFS results of Abbate *et al* [28] also allows one to rule out VO_2 and, although poorly resolved, not only the energy position but also the multiplet structure suggest that the post-oxidation films of Price *et al* [27] are indeed V_2O_3. Interestingly, although the sample preparation conditions of this work are not very dissimilar to those of Sambi *et al* [26], the results are in striking contrast with purely V_2O_3 films formed while the latter claimed VO_2 and V_2O_5. Presumably, subtle differences in sample preparation lead to these differences and, given that V_2O_3 is formed by reactive evaporation (see later), the substrate surface oxygen must be playing a decisive role in the formation of higher oxides.

Evaporation of vanadium in an oxygen partial pressure results in vanadia deposition on TiO_2. Both XPS and NEXAFS indicate that only V_2O_3 is formed from submonolayer to multilayer coverages. The Ti L-edge features show only a smooth attenuation with increasing V-oxide coverage indicating vanadia deposition does not significantly disturb the structure of the TiO_2 support [29], unlike the metallic vanadium deposition [27]. A useful aspect of NEXAFS is its ability to highlight the interface by comparison of data taken in total yield mode with that obtained in the more surface-sensitive Auger yield mode. The V L-edge spectra grow with increasing coverage with no energy shifts or significant line shape change although the characteristic V_2O_3 multiplet structure only becomes well expressed beyond 1 ML coverage. The smooth Ti edge attenuation and V edge growth was attributed to a simultaneous multilayer growth mode. The thin V_2O_3 multilayer films were found to be stable up to 1100 K in UHV, however, a structural rearrangement could be observed by NEXAFS beyond this temperature. At 1150 K the integrated Ti L-edge intensity increased by approximately a factor of five although the V L-edge intensity decreased only slightly. This was attributed to the formation of larger vanadia particles rather than the interdiffusion or encapsulation by titania, as no reduced TiO_x was evident. The subtle changes in the Ti L-edge features associated with the Ti 3d-e_g orbitals were interpreted in terms of a change from a tetragonal rutile coordination at the interface to a more symmetric cubic or trigonal environment. The small shift (0.3 eV) to lower energy of the V L-edge features on heating was suggested to be the result of the formation of $VTiO_3$ mixed oxide at the interface.

A similar combined XPS and NEXAFS investigation of reactive evaporation of vanadium onto the catalytically inactive Al_2O_3 substrate was also undertaken by Biener *et al* [30]. The conclusions were essentially the same as on the TiO_2 substrate—a stable V_2O_3 oxide is formed displaying a simultaneous multilayer growth mode. In this investigation the pitfalls inherent in using XPS binding energies to determine chemical state are exemplified. On increasing V-oxide deposition XPS shifts of over one eV were observed for both O 1s and V 2p emissions relative to the substrate Al emissions, which in turn shifted substantially with coverage. In contrast the V edge NEXAFS spectra show neither a shift in energy or change in lineshape from that of V_2O_3. The behaviour of the XPS was thus attributed to both final state effects and charging, the latter varying with deposition of the conducting V_2O_3 film.

Biener *et al* [29, 30] have concluded that since V_2O_3 appears to be the stable oxide formed, despite V_2O_5 being the thermodynamically stable oxide, higher oxidation states must be kinetically hindered. Moreover, as the same oxide is produced on both catalytically active (TiO_2) and inactive (Al_2O_3) substrates they suggest the function of the support is not to generate a specific vanadium oxide but rather to participate as an active part of the catalytic reaction, in line with the ideas of 'monolayer catalysts'.

In the class of so-called monolayer-type catalysts the spreading of the metal oxide plays an important role in their preparation. Recently, this has been investigated by photoemission spectromicroscopy (SPEM): laterally resolved, quantitative XPS [31, 32]. In the Al_2O_3 supported Mo–oxide industrial catalyst the support oxide powder (Al_2O_3) is mixed with MoO_3

crystals which, after annealing in humid oxygen, homogeneously wet the support surfaces with a monolayer of Mo–oxide. The system used to model this spreading was an *ex situ* heat-treated, anodically oxidized polished Al foil with a 20 nm thin polycrystalline oxide film, on which small MoO_3 crystals were placed. In the SPEM the monochromated photon beam was focussed to a submicrometre spot by a zone plate optical system. In the imaging mode photoemission features of chosen kinetic energies are collected while scanning the sample. The images in this study where created from raw images of the Al 2p of the support, a secondary electron background and Mo 3d emissions from the MoO_3 crystallites and the spreading Mo–oxide phase. The latter two were energetically separated by both chemical shifts (the photon beam caused reduction of the monolayer oxide) and differential charging effects. Typical processed images of a $60 \times 60\ \mu m^2$ area are displayed in figure 12. It should be noted that despite the oxygen treatment steps being performed *ex situ* the SPEM could be reproducibly realigned with the aid of an optical microscope. The monolayer oxide XPS emission intensity provides the bright contrast and the spreading of the oxide with increasing annealing times in dry oxygen is well expressed. After prolonged treatment the original MoO_3 crystals completely disappear and a homogeneous monolayer Mo–oxide results. The spreading can be quantified with the Mo 3d Al 2p XPS intensity ratio. Significantly, it was found that in the initial stages of spreading the coverages were always below that of the final monolayer. This was argued to imply that the Mo–oxide spreads by a diffusion process rather than the hitherto favoured so-called carpet unrolling mechanism. In the latter it is assumed that the Mo is only mobile on top of MoO_3 and the already wet support and a coverage of greater than 1 ML would be expected to be found spreading out from the MoO_3 crystals, which was quite clearly not the case. The quantification afforded by the SPEM also allowed the determination of an effective diffusion constant and experiments are planned to clarify whether it is surface diffusion or diffusion via gas phase transport [32].

5. Metals on metals: heterogeneous bimetallic surfaces

A metal single crystal surface partly covered with islands of a different metal constitutes an interesting model system to investigate locally different adsorption properties coexisting at the same surface. The laterally inhomogeneous surface may form an inhomogeneous distribution of adsorbate species and the diffusion processes between the different parts of the surface, which are driven by the differences in the adsorption strength, may lead to inhomogeneous reactivity patterns. The physical, chemical and catalytic properties of bimetallic surfaces have been reviewed recently by Rodriguez [33].

High resolution core level spectroscopy is particularly well suited to study molecular adsorption on heterogeneous bimetallic surfaces, because the adsorbed species on the different metal patches can be distinguished by their different core level binding energies and the corresponding surface coverages can be evaluated quantitatively. This approach has been successfully demonstrated by Beutler *et al* [34] for CO-exposed Rh(111) surfaces, which have been decorated with two-dimensional Pd island structures. It is shown that coverage-dependent diffusion processes between the Pd and Rh surface parts have a significant influence on the lateral distribution of CO molecules on the surface.

Figure 13(a) shows Pd $3d_{3/2}$ spectra for 0.5 ML Pd/Rh(111), clean and exposed to different amounts of CO. Note that the Pd 3d spectra exclusively monitor the adsorption on the Pd islands. On the CO-exposed surfaces below saturation coverage the clean surface component at 335.35 eV BE and a CO-induced component at higher BE coexist in the spectra, but at CO saturation (10 L exposure) all Pd atoms are influenced by the bonding to CO and the CO-induced component is at 335.75 eV BE, whereas the clean surface component

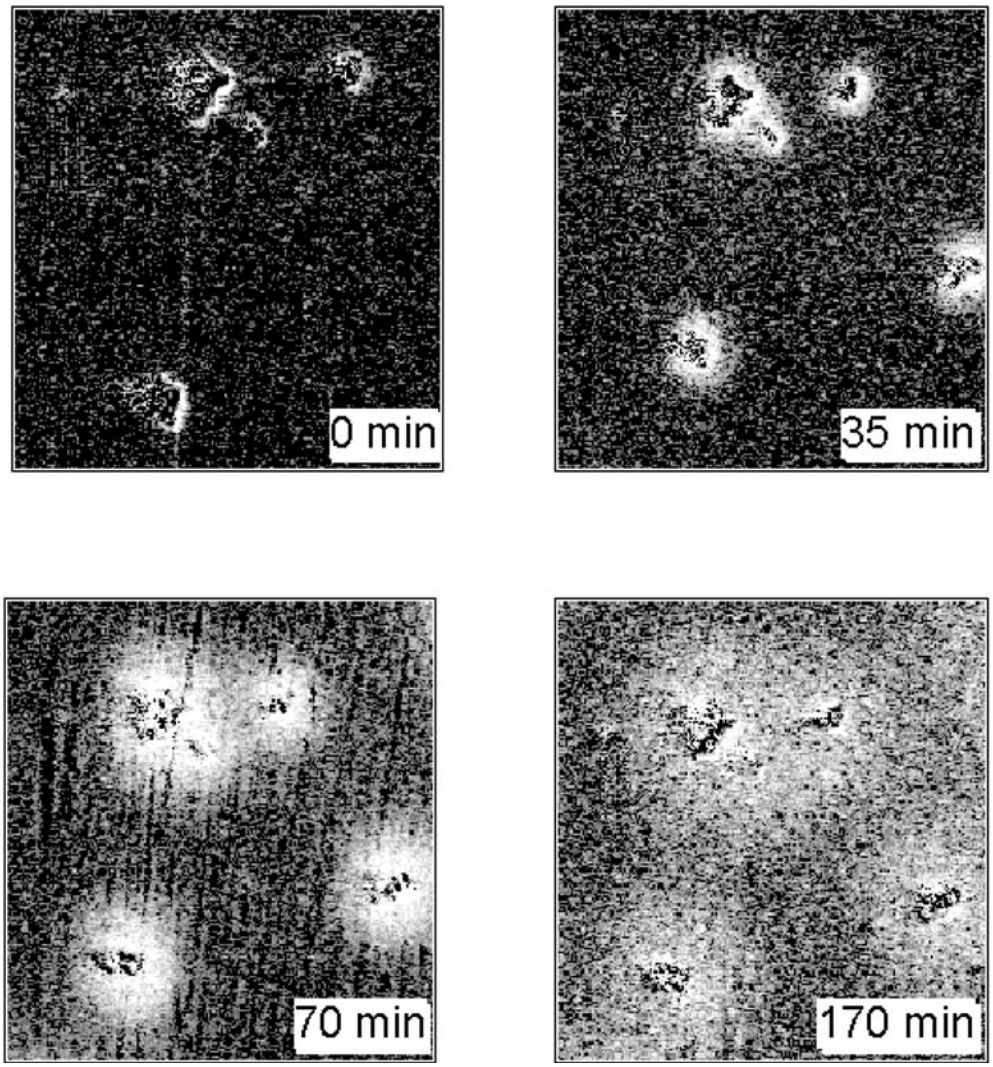

Figure 12. SPEM chemical maps showing the spreading from MoO_3 crystals over a model Al_2O_3 support induced by annealing in dry oxygen at 630 K for the given times. Image size = 60 × 60 μm, hν = 600 eV, lateral resolution = 0.15 μm. From [32] with permission.

has vanished completely. After annealing the sample to 400 K the clean surface spectrum is restored (figure 13(a), top spectrum) indicating that all CO has left the Pd islands. A quantitative comparison of spectra between the partially Pd-covered (0.5 ML Pd) and a fully Pd-covered (1 ML Pd) Rh(111) surface with respect to the exact CO exposure values reveals that the exposures required to induce a particular relative intensity of the CO-induced Pd $3d_{3/2}$ component are significantly higher on the mixed 0.5 ML Pd/Rh(111) surface than on the 1 ML Pd/Rh(111) surface. In other words, the CO coverage on the Pd islands of a mixed Pd Rh surface is lower for a given exposure (below saturation coverage) than on a homogeneously Pd-covered Rh surface.

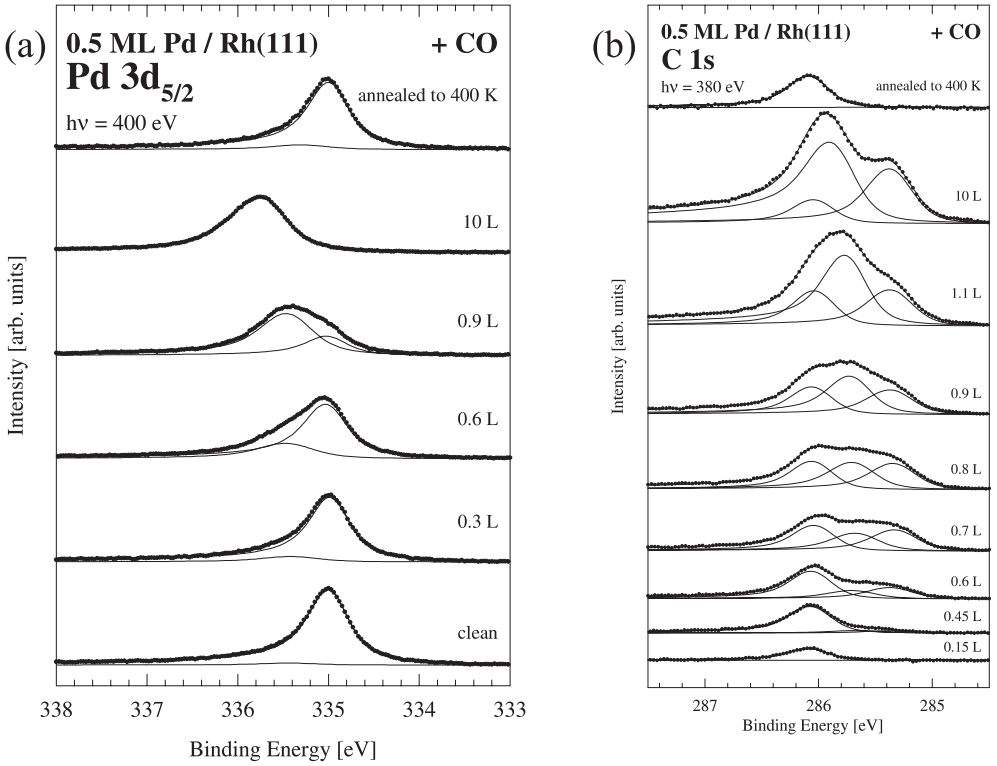

Figure 13. (a) Pd $3d_{3/2}$ spectra and their decomposition at different CO exposures on 0.5 ML Pd/Rh(111) and after annealing a CO-saturated surface to 400 K. (b) C 1s spectra and their decomposition at different CO exposures on 0.5 ML Pd/Rh(111) and after annealing the CO-saturated surface to 400 K. From [34] with permission.

The C 1s spectra give information on the CO adsorption on the whole surface, i.e. on both the Pd islands and the bare Rh areas (figure 13(b)). Using the C 1s spectra of CO on Rh(111) and on 1ML Pd/Rh(111) as guidance, the spectra of figure 13(b) may be decomposed into three components, two corresponding to the CO adsorbed on Rh in the on-top and hollow sites and one on the Pd sites. Notably, at low exposures ($\leqslant$0.45 L) CO adsorption is detected at Rh sites only, in accordance with the results of the Pd 3d spectra. After annealing the CO-saturated surface to 400 K only one peak remains in the C 1s spectrum, which has been associated with CO in on-top sites on Rh(111), thus demonstrating that all CO has desorbed from the Pd islands. Beutler *et al* [34] have concluded that the CO molecules populate exclusively the Rh(111) parts of the surface at low CO exposures and that an efficient diffusion from the Pd islands to the Rh(111) areas takes place. At higher exposures the population of the Pd island surfaces is initiated and a reverse diffusion current of CO from Rh to Pd takes place. It has been suggested that the driving force for these diffusion processes is the coverage-dependent variation of the CO adsorption energies on the two parts of this heterogeneous surface.

Another interesting example worth mentioning in the present context is provided by the work of Jaworowski *et al* [35], who have studied the dissociation of NO on a Pd(100) surface which was decorated partially by c(2 $\times$ 2)-PdMn alloy structures. It has been found that the adsorption of NO on the alloy destroyed the ordered c(2 $\times$ 2) phase and that the dissociation of NO takes place upon heating, which is in contrast to NO on the clean Pd(100) surface, from where NO desorbs intact. Furthermore, the dissociation process on the heterogeneous mixed

PdMn-c(2×2)/Pd(100)-(1×1) surface showed differences to a single phase PdMn-c(2×2) alloy surface in terms of a dissociation activity at higher temperature. It has been conjectured that the Pd atoms at the boundaries of the alloy islands play an active role for NO dissociation, albeit at higher temperature. Jaworowski *et al* [35] speculated about the validity of such a PdMn-Pd bifunctional surface for the reduction of NO by CO, where 'NO-dissociation centres' at the alloy boundaries are separated by clean Pd(100) areas, which are efficient for the oxidation of CO by adsorbed oxygen.

6. Oxide-decorated metal surfaces

Metal single crystal surfaces decorated by submonolayer quantities of an oxide phase constitute a system which can be conceptually regarded as an 'inverse or inverted' model catalyst. This model system contains the important metal–oxide interface and oxide–metal phase boundaries, and possible active sites associated with them. Thus, the influence of the metal–oxide interface on the physico-chemical properties of this heterogeneous system may be focussed upon, and complementary information to that from real catalyst model systems, discussed in section 3, may be obtained. The V-oxide/Pd(111) system has been chosen here to illustrate the application of synchrotron radiation for the characterization of 'inverse' model catalysts. This system has been extensively studied in our group over the past years by a number of surface-sensitive techniques, including LEED, STM [36-39], high-resolution XPS and NEXAFS using synchrotron radiation [36, 40, 41], and high-resolution electron energy loss spectroscopy (HREELS) [42].

The important issues of the oxide-on-metal systems are

(i) structure and morphology of the ultrathin oxide phases,
(ii) stoichiometry and oxidation state,
(iii) thermal behaviour and
(iv) the chemical properties of the oxide decorated metal surfaces.

6.1. V-oxide film characterization

The V-oxide on Pd(111) inverse catalyst surfaces have been fabricated by deposition of vanadium metal at 250 °C in 2×10^{-7} mbar of oxygen onto the clean Pd(111) surface. Figure 14 shows V $2p_{3/2}$ core-level photoemission spectra (a), V L-edge (b), and O K-edge (c) NEXAFS spectra of V-oxide on Pd(111) for increasing film thickness (in MLE) [36]. For thick (∼5 MLE) V-oxide films both XPS and NEXAFS spectra exhibit the characteristic features of bulk-type V_2O_3. The V $2p_{3/2}$ core level spectrum (top spectrum, figure 14(a)) consists of a single component with a binding energy of 515.4 eV, which is close to the values of 515.7 and 515.8 eV cited in the literature for V_2O_3 [43–45]. The V L-edge NEXAFS spectrum of 5 MLE V-oxide (figure 14(b), top spectrum) is characterised by two near-edge features at 517.0 and 523.5 eV, which are related to excitations of electrons from the V $3p_{3/2}$ (L_{III}-edge) and V $3p_{1/2}$ (L_{II}-edge) orbitals into empty or partially occupied vanadium 3d states, respectively [12]. The overall shape and the energy positions of the L_{III}-and L_{II}-transitions resemble very closely those reported by Abbate *et al* [28] and Chen [12] for V_2O_3, supporting the XPS result. The corresponding O K-edge NEXAFS spectrum (figure 14(c), top spectrum) can be assigned to transitions from the O 1s core level to unoccupied states in the conduction band. The ligand field causes the V 3d band to split into two sublevels at 530.6 (t_{2g}) and 532.5 eV (e_g). The observed ligand field splitting is close to the value of 2.2 eV reported for vanadium oxides [46] and indicates an octahedral oxygen coordination of the vanadium

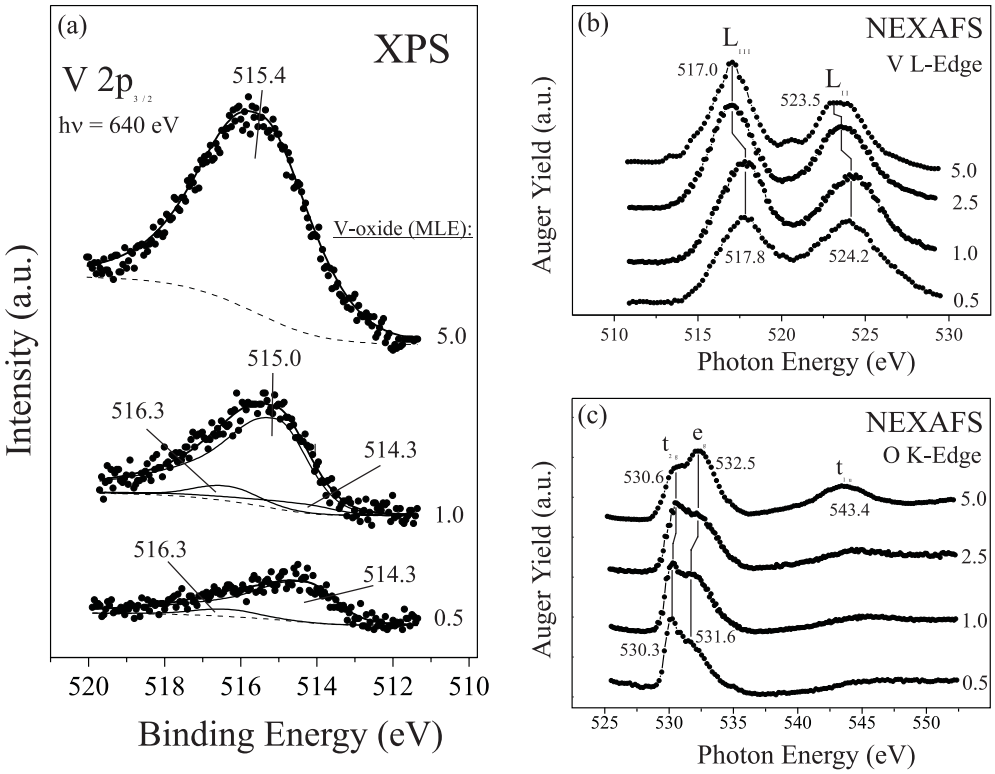

Figure 14. (a) Normal emission V $2p_{3/2}$ core-level spectra for different vanadium oxide coverages on Pd(111). (b) Vanadium L-edge and (c) oxygen K-edge NEXAFS spectra for various oxide thicknesses.

cations. The broad structure at 543.4 eV (t_{1u}) arises from transitions into empty or partly occupied V 4sp states. The intensity of the t_{2g} resonance is smaller than the e_g-related signal and if compared to NEXAFS spectra of V_2O_5, VO_2, and V_2O_3 indicates the presence of a partially filled t_{2g} band [28]. Again, the O K-edge spectrum is consistent with the formation of V_2O_3.

At 1 MLE the V $2p_{3/2}$ XPS spectrum (figure 14(a), middle spectrum) is dominated by a component with a binding energy of 515.0 eV, which coexists with two minor components at 514.3 and 516.3 eV. The major component at 515.0 eV is presumably due to a thin layer of a V_2O_3-like phase, whose V $2p_{3/2}$ binding energy is shifted by about 0.4 eV to lower BEs with respect to bulk V_2O_3, due to the proximity of the underlying metal surface [36]. The minor component at 516.3 eV has been associated with the existence of VO_2, by comparison with the literature value of 516.2 eV for bulk-type VO_2 at room temperature [43, 44]. The identification of the other minor component with a BE of 514.3 eV will be discussed later. The heterogeneous character of the as-grown monolayer oxide surface has been confirmed by STM measurements, which have shown that the V-oxide films on Pd(111) exhibit a complex morphology, consisting of oxide islands with different surface structures [37, 38]. In the V L-edge NEXAFS spectrum (figure 14(b)) the L_{III} and L_{II} transitions shift by about 0.7 eV to higher photon energies between 5 and 1 MLE which, according to the calibration performed by Chen *et al* [47], corresponds to a change of the V oxidation state from 3+ to 4+, i.e. the formation of a VO_2-like phase. On the other hand, the line shapes of both V L-edge and O K-edge spectra at 1 MLE, though distinctly different to V_2O_3, disagree with the respective

x-ray absorption spectra for the rutile VO_2 phase, as published by Abbate *et al* [28]. The t_{2g} and e_g features in the O K-edge spectrum (figure 14(c)) shift to 530.3 and 531.6 eV, respectively, with the ligand field splitting decreasing to about 1.3 eV, indicating that the octahedral environment of V cations is distorted in the 1 MLE phase. This is consistent with the formation of a mixture of different V oxide phases, as observed by XPS and STM [38], which results in a variation of the interatomic distances and hence in the amount of hybridization. The latter will influence the t_{2g} versus e_g intensity distribution and also the ligand field splitting.

At 0.5 MLE the component at 514.3 eV becomes dominant in the V $2p_{3/2}$ core level spectrum (figure 14(a), bottom spectrum). This component has been initially identified as due to a VO-like phase with an oxidation state of 2+, since it is located between the V_2O_3 peak at 515.4 (oxidation state 3+) and the metallic vanadium BE of 513.2 [36]. STM measurements have demonstrated, however, that the as-grown 0.5 MLE V-oxide/Pd(111) surface is composed of a two-dimensional (2D) porous overlayer with a locally ordered $p(2 \times 2)$ honeycomb structure and second layer islands with a different structure [37]. *Ab initio* density-functional theory (DFT) calculations have revealed that the honeycomb structure corresponds to a new interface-stabilized surface V-oxide phase with a formal V_2O_3 stoichiometry (s-V_2O_3) [37]. This s-V_2O_3 layer consists of a hexagonal V layer in fcc and hcp three-fold hollow Pd(111) sites and of bridging oxygen atoms forming the outer oxide surface. It has been suggested that the direct contact between the V atoms and the Pd(111) surface causes the s-V_2O_3 component to appear at a binding energy (514.3 eV), i.e. shifted by about 1 eV with respect to the binding energy of bulk-type V_2O_3 phase (515.4) [37]. The minor VO_2-like component at 516.3 eV can be associated with the second layer islands seen in the STM images [37, 38]. In the O K-edge NEXAFS spectrum at 0.5 MLE the intensity ratio of the t_{2g}/e_g features increases when compared to the 1 MLE case, while no significant differences are observed in the V L-edge spectra.

In order to test the thermal stability of the V-oxide films on Pd(111) annealing treatments up to 500 °C in vacuum have been performed. The thermal behaviour of one-monolayer-thick V-oxide layers is of special interest, since at this coverage vanadium oxide islands and free palladium patches still coexist at the surface. This forms an appropriate model system for studying the effects of the metal–oxide phase boundary on the reactivity, which is an important problem in catalysis. Figure 15(a) shows the evolution of V $2p_{3/2}$ core-level XPS spectra of 1 MLE V-oxide after the evaporation at 250 °C and the annealing at different temperatures. After annealing at 300 °C two spectral components at 516.3 eV and 514.3 eV BE coexist in the spectra, due to VO_2 and s-V_2O_3 phases, respectively. Some bare Pd patches have also been detected on this surface with STM and CO titration experiments. The atomically resolved STM image in figure 15(b) shows that the honeycomb (2×2) s-V_2O_3 layer coexists with two types of V-oxide islands, with rectangular and hexagonal symmetries. The latter have been associated with formal VO_2 stoichiometries, which exhibit rectangular (VO_2-rect) and hexagonal (VO_2-hex) structures [38, 39]. It is important to note that both VO_2-rect and VO_2-hex phases represent interface-stabilized metastable phases and not the stable bulk-type rutile VO_2 lattice. They exist only in a narrow coverage range around 1 MLE and converge gradually to the bulk V_2O_3 phase with increasing oxide thickness [39].

Annealing to 350 °C in vacuum causes a reduction of the V-oxide films, as evident from the dominant character of the s-V_2O_3 component in the V $2p_{3/2}$ XPS spectrum. The surface is now completely covered by the s-V_2O_3 layer, as revealed by STM measurements. Further annealing to 500 °C results in the decomposition of the oxide and the formation of metallic vanadium and a V/Pd alloy, as evident from the XPS components at 513.2 eV and 513.6 eV BE, respectively. The formation of a well-ordered V/Pd surface alloy is also observed in STM

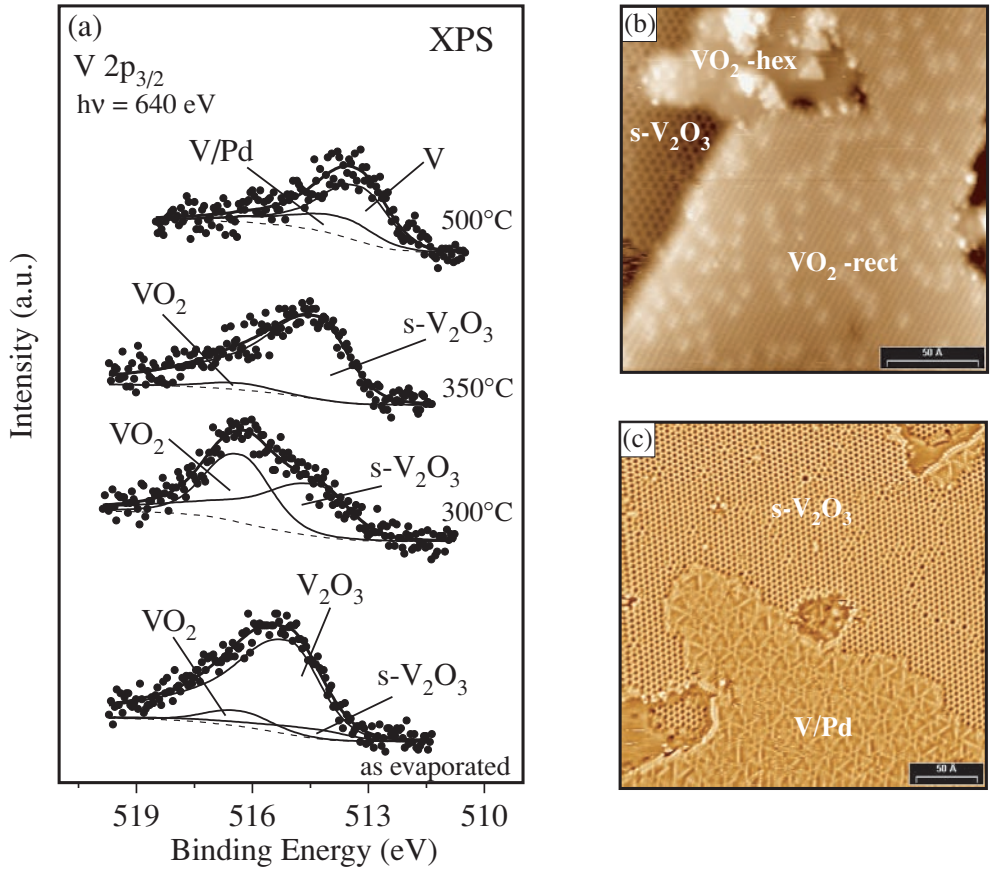

Figure 15. (a) V $2p_{3/2}$ core-level photoemission spectra for 1 MLE V-oxide as a function of the annealing temperature. (b) STM images of the 1MLE V-oxide film annealed in vacuum to 300 °C (200 Å × 200 Å, 0.25 V; 0.5 nA) and (c) 400 °C (300 Å × 300 Å, 0.1 V; 1.0 nA).

in the form of 2D islands with a characteristic 'wagon wheel' network structure (figure 15(c)). At 400 °C these V/Pd islands coexist with the s-V_2O_3 layer, while at 500 °C only metallic V and V/Pd islands are detected.

The thermal stability of the V-oxide films has been found to be coverage dependent [36]. After heating 2.5 MLE oxide films to 500 °C only the V/Pd alloy component is left in the V $2p_{3/2}$ core level spectrum (figure 16(a)): all oxide has decomposed. For 5 MLE thick oxide the major constituent after the annealing to 500 °C is still V_2O_3, but some oxide has decomposed into the alloy phase. This is corroborated by the STM image shown in figure 16(b), where three-dimensional islands with the bulk-type V_2O_3 corundum structure coexist with flat areas exhibiting the 'wagon wheel' pattern due to the V/Pd surface alloy phase. The complete reduction of the 5 MLE V_2O_3 phase requires higher temperature of 700 °C. The XPS spectra of the heated 2.5 MLE films still reveal the presence of oxygen on the surface (see inset of figure 16(a)), possibly in the form of chemisorbed oxygen on the alloy surface. This interpretation is supported by the corresponding O K-edge NEXAFS spectrum (figure 17(b)), where the V 3d-related band region is dominated by a single feature at a photon energy of 530.6 eV, indicating a significant weakening of the ligand field due to the oxide decomposition. The strong feature at 530.6 eV can thus be attributed to the chemisorbed

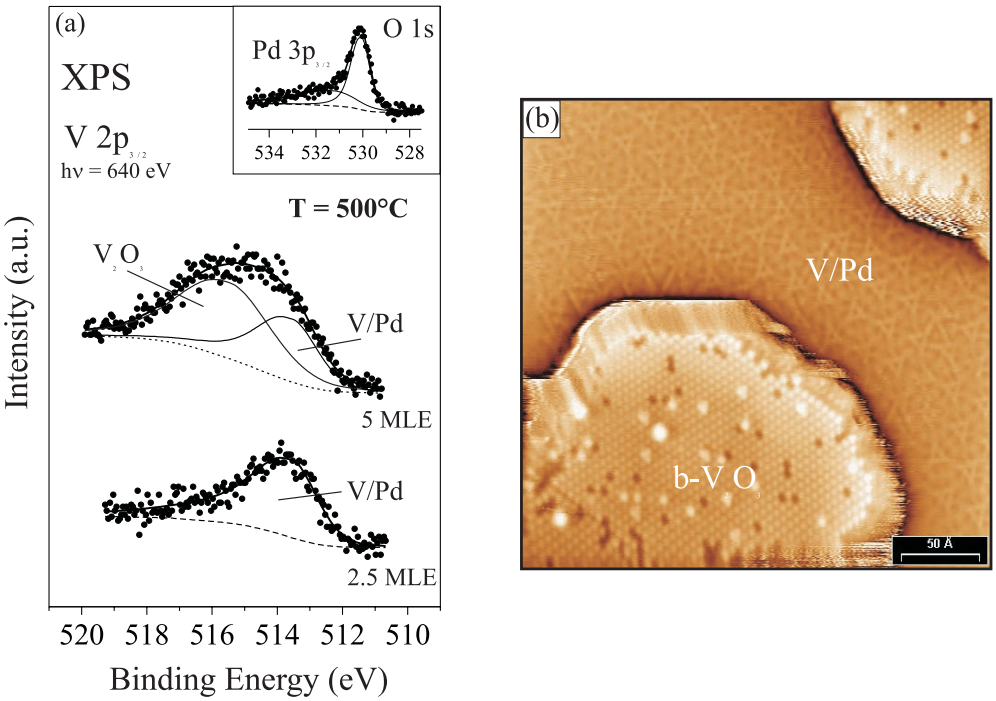

Figure 16. (a) V $2p_{3/2}$ core-level photoemission spectra for 2.5 MLE and 5 MLE thick V-oxide layers annealed to 500 °C in vacuum. The insert shows the O 1s spectrum taken after annealing the 2.5 MLE film to 500 °C. (b) STM image (300 Å × 300 Å, 0.5 V; 0.3 nA) of the 5 MLE V-oxide film annealed to 500 °C in vacuum.

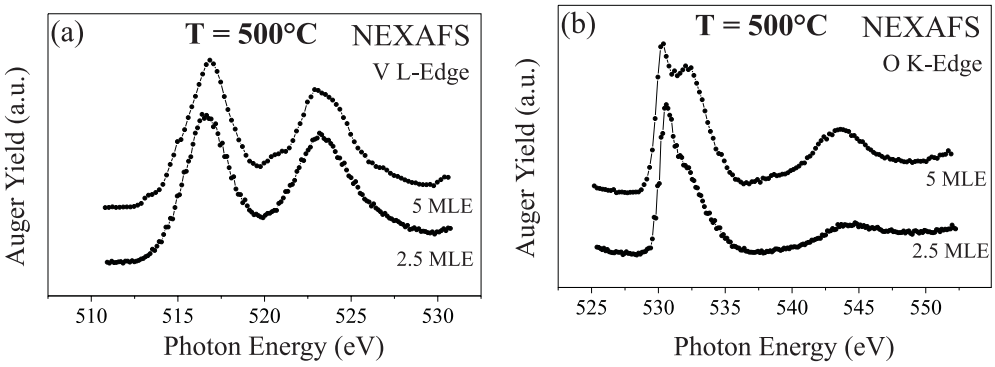

Figure 17. (a) V L-edge and (b) O K-edge NEXAFS spectra for 2.5 MLE and 5 MLE V-oxide layers after annealing to 500 °C in vacuum.

oxygen, while the weak shoulder at 532.3 eV and the broad structure at 544.3 eV are possibly due to some oxide remainders at 2.5 MLE, which are not resolved in the XPS spectrum. The 5 MLE O K-edge spectrum can be regarded as a mixture of V_2O_3 and chemisorbed oxygen phases, in agreement with the XPS result. In the V L-edge NEXAFS spectra (figure 17(a)) the L_{III} transition of the 2.5 MLE film shifts by about 0.4 eV to lower photon energies on annealing, confirming the oxide reduction, while only minor changes in the V_2O_3 lineshape of the 5 MLE L-edge spectra are observed after annealing at 500 °C.

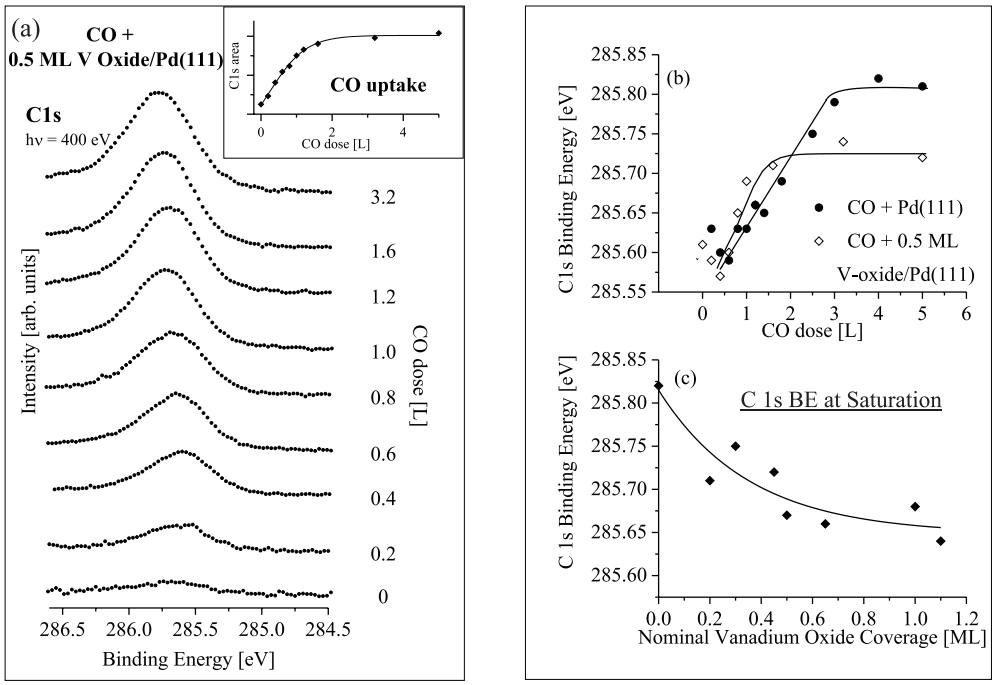

Figure 18. (a) C 1s XPS spectra of CO adsorbed on the 0.5 MLE V-oxide/Pd(111) surface, as a function of the CO dose. The insert shows the C 1s peak area versus CO dose (CO uptake curve). (b) C 1s binding energy versus CO dose for the clean Pd(111) and 0.5 MLE V-oxide/Pd(111) surfaces. (c) C 1s binding energy at CO saturation on V-oxide/Pd(111) surfaces versus nominal V oxide coverage. From [41].

6.2. Adsorption of CO

The adsorption of CO at room temperature on the V-oxide/Pd(111) 'inverse catalyst' surfaces has been investigated by Leisenberger *et al* [41] employing high resolution XPS with synchrotron radiation. CO is widely used as a probe molecule for heterogeneous surfaces since it provides a good test case for the modifications of the electron distribution of surface sites. Since CO does not chemisorb on vanadium oxide at room temperature [40], it is well-suited as a molecular probe of the Pd sites at the V-oxide/Pd(111) interface. Figure 18(a) displays a sequence of C 1s core level spectra of CO on 0.5 MLE V-oxide/Pd(111) as a function of CO exposure at room temperature. The C 1s binding energy is observed at ∼285.6 eV at low CO coverage and it increases to ∼285.72 eV for CO saturation coverage. The inset shows a plot of the C 1s areas versus CO exposure for the spectra in figure 18(a), which yields the CO uptake curve for the 0.5 MLE oxide/Pd(111) surface.

In figure 18(b) the C 1s binding energies are plotted against the CO dose for the clean Pd(111) and for the 0.5 MLE V-oxide/Pd(111) surface. Two significant differences can be observed: (i) the BE value at CO saturation is lower for the oxide-covered surface, and (ii) the CO saturation adsorption is reached at lower CO exposures on the V-oxide/Pd(111) than on the clean Pd(111) surface. The C 1s binding energies at CO saturation are plotted as a function of the V-oxide coverage in figure 18(c). They decrease smoothly with oxide coverage, the range of variation being ∼200 meV. The C 1s BE of CO adsorbed on a particular metal surface has been shown to be dictated primarily by the adsorption site [15, 48, 49]. The C 1s XPS core

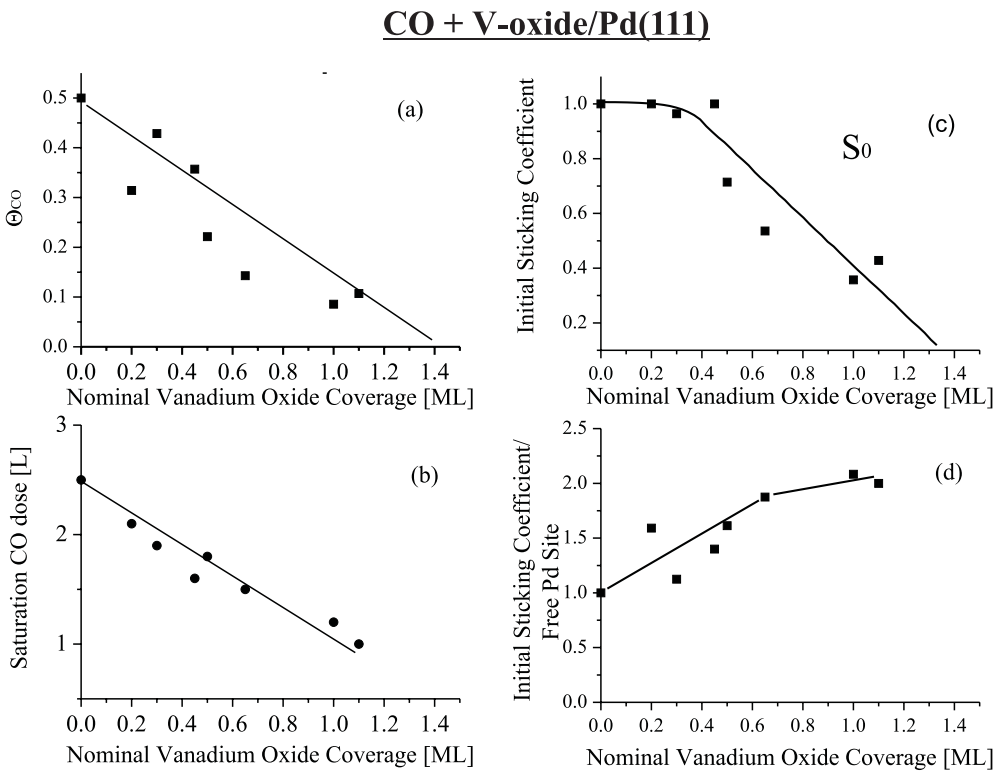

Figure 19. Plots of (a) the CO coverage, (b) the CO exposure to reach saturation adsorption conditions, (c) the overall initial sticking coefficient of CO, and (d) the initial sticking coefficient per free Pd site on V-oxide/Pd(111) surfaces versus nominal V oxide coverage. From [41].

level spectra for CO adsorption on Pd(111) at room temperature have been measured recently at very high resolution by Surnev *et al* [17]. The peak decomposition analysis performed in this work revealed that the C 1s peaks needed two spectral components for CO coverages (Θ_{CO}) exceeding 0.1 ML to obtain a good fit: one component at ∼285.55 eV, which is attributed to the adsorption of CO in three-fold hollow sites, and a second component at ∼285.8 eV, associated with the occupation of bridge sites. The CO adsorption in three-fold hollow sites in the $(\sqrt{3} \times \sqrt{3})$R30° structure prevails for CO coverages up to 0.33 ML, while between 0.33 ML and 0.5 ML (the saturation coverage of CO on Pd(111) at 300 K) progressive population of bridge sites takes place. The latter sites are considered to form domain boundaries in a poorly ordered $(\sqrt{3} \times \sqrt{3})$R30° phase [17]. Following this line of thought Leisenberger *et al* [41] suggested that the presence of the V-oxide phase on the Pd(111) surface shifts the balance between the bridge and hollow sites with increasing CO density on the surface. As the oxide coverage increases and the areas of the free Pd sites decrease, the number of CO domain boundaries decrease because the metal-oxide interface provides new boundary conditions. The increasing population of hollow sites at the expense of bridge sites would then lead to the observed reduction (or absence) of a C 1s BE shift as a function of Θ_{CO}, with increasing oxide coverage (figure 18(c)). An alternative explanation could be that the CO molecules adsorbed at or near the oxide–metal phase boundary prefer higher coordination sites.

Figure 19 demonstrates that the oxide phase influences not only the adsorption site distribution but also the adsorption kinetics of CO on V-oxide/Pd(111) surfaces. In

figure 19(a) the CO surface coverage at saturation is plotted against the nominal V-oxide coverage: there is an approximately linear decrease of Θ_{CO} as a result of the blocking of Pd sites by the oxide phase. In figure 19(b) the CO saturation exposure, i.e. the exposure necessary to reach saturation adsorption conditions, decreases as well with increasing oxide coverage. This is unexpected, since the saturation exposure for adsorption on the free Pd areas should not be a function of the oxide coverage, unless the oxide phase plays a kinetic role in the CO adsorption process, which seems to be the case. This suggests that CO, adsorbed on the V-oxide surface in an intermediate mobile precursor state, spills over the oxide–metal phase boundary and diffuses on to free Pd sites, where it chemisorbs. Thus the 'inverse catalyst' considered here mimics supported catalyst systems where diffusion of CO over an oxide support to reach metal particles has also been reported [50]. The initial sticking coefficient per free Pd site (figure 19(d)), which is obtained by renormalizing the sticking coefficient data of figure 19(c) to the number of free Pd sites using figure 19(a), increases with the V-oxide coverage and reaches a value of $\sim$2 at 1 MLE oxide. This is incompatible with the classical definition of the initial sticking coefficient, but is a clear manifestation of the spillover effect: the oxide surface provides an additional source of CO and the initial sticking coefficient formally increases beyond unity.

7. Outlook

Synchrotron radiation-based methods will remain at the forefront of experimental techniques for the characterisation of model catalyst surfaces. The heterogeneous nature of these systems requires techniques which give information on a local scale. The latter is inherently included in the x-ray microscopy techniques with their imaging capabilities, and the inclusion of local spectroscopy in the spectromicroscopy method opens new possibilities of characterisation with geometric and chemical information obtainable from the same small area. The increasing importance of x-ray microscopy methods is therefore easily foreseen as a future focus. But even more conventional core level spectroscopies such as x-ray photoelectron spectroscopy, if the resolution is high enough, are suitable probes for heterogeneous surfaces, if, for example, the sensitivity of surface core level shifts to adsorbate species is employed to detect local differences in adsorbate behaviour. The very high resolution obtainable nowadays in core level spectra recorded at third generation synchrotron radiation sources also allows one to resolve the vibrational finestructure in the core level photoemission signals of adsorbed species, and this provides additional means for the identification of molecular fragment species, which may occur as intermediates in a catalytic reaction.

X-ray absorption structure already plays an important role in combination with XPS particularly for thin oxide films. Structural probes such as the surface-extended x-ray absorption fine structure (SEXAFS) and photoelecton diffraction have only occasionally been used to study catalyst model systems, but they have potential which will certainly be exploited further in the future. Very recently, grazing incidence small-angle x-ray scattering (GISAXS) has been applied to study the morphology of growing islands of Pt, Pd and Ag on a MgO(001) substrate [51]. This new technique allows one to study the growth dynamics of metal islands *in situ* in UHV in real time, but it also has in principle the potential to be applied at higher pressure ambients.

The model catalyst systems mentioned here have essentially been attempting to bridge the 'materials gap' to real catalysts, the next non-trivial challenge will be to bridge the 'pressure gap' with these models. The investigation of model catalyst surfaces under high pressure reaction conditions is another cutting-edge area of catalytic research, where synchrotron radiation-based techniques will play an important role. First experiments using

x-ray absorption spectroscopic techniques have been reported, where the electronic structure of a working catalyst under dynamic conditions at high pressures has been determined [52]. High pressure studies on model catalysts with the use of synchrotron radiaton are only in the infancy at the present time, but we expect a bright future for these methods in the times to come.

Acknowledgments

We acknowledge the financial support of the Austrian Science Foundation within the framework of the Joint Research Programme 'Gas-Surface Interactions'.

References

[1] Somorjai G A and Yang M X 1997 *J. Mol. Catal.* A **115** 389
[2] Gunter P L J, Niemandsverdriet J W H, Ribeiro F H and Somorjai G A 1997 *Catal. Rev.-Sci. Eng.* **39** 77
[3] Goodman D W 1994 *Surf. Rev. Lett.* **1** 449
[4] Ertl G and Freund H-J 1999 Physics Today, January p 32
[5] Kuhlenbeck H and Freund H-J 1997 *Growth and Properties of Ultrathin Epitaxial Layers, The Chemical Physics of Solid Surfaces* ch 9 ed D A King and D P Woodruff (New York: Elsevier) p 340
[6] Kuhlenbeck H, Odörfer G, Jaeger R, Illing G, Menges M, Mull Th, Freund H-J, Pöhlchen M, Staemmler V, Witzel S, Scharfschwerdt C, Wennemann , Liedtke T and Neumann M 1991 *Phys. Rev* B **43** 1969
[7] Mullins D R, Radulovic P V and Overbury S H 1999 *Surf. Sci.* **429** 186
[8] Cai Y Q, Bradshaw A M, Guo Q and Goodman D W 1998 *Surf. Sci.* **399** L357
[9] Tauster S J, Fung S C, Baker R T K and Horsley J A 1981 *Science* **211** 1121
[10] Biener J, Bäumer M, Wang J and Madix R J 2000 *Surf. Sci.* **450** 12
[11] Stöhr J 1992 *NEXAFS Spectroscopy (Springer Series in Surface Sciences)* (Berlin: Springer)
[12] Chen J G 1997 *Surf. Sci. Rep.* **30** 1
[13] Sandell A, Libuda J, Brühwiler P, Andersson S, Maxwell A, Bäumer M, Mårtensson N and Freund H-J 1995 *J. Electron Spectr. Relat. Phenom.* **76** 301
[14] Bäumer M and Freund H-J 1999 *Prog. Surf. Sci.* **61** 127
[15] Björneholm O, Nilsson A, Tillborg H, Bennich P, Sandell A, Hernnäs B, Puglia C and Mårtensson N 1994 *Surf. Sci.* **315** L983
[16] Ramsey M G, Leisenberger F P, Netzer F P, Roberts A J and Raval R 1997 *Surf. Sci.* **385** 207
[17] Surnev S, Sock M, Ramsey M G, Netzer F P, Wiklund M, Borg M and Andersen J N 2000 *Surf. Sci.* **470** 171
[18] Tillborg H, Nilsson A and Mårtensson N 1993 *J. Electron Spectr. Relat. Phenom.* **62** 73
[19] Sandell A, Libuda J, Brühwiler P A, Andersson S, Maxwell A J, Bäumer M, Mårtensson N and Freund H-J 1996 *J. Vac. Sci. Technol.* A **14** 1546
[20] Frank M, Andersson S, Libuda J, Stempel S, Sandell A, Brena B, Giertz A, Brühwiler P A, Bäumer M, Mårtensson N and Freund H-J 1997 *Chem. Phys. Lett.* **279** 92
[21] Frank M, Andersson S, Libuda J, Stempel S, Sandell A, Brena B, Giertz A, Brühwiler P A, Bäumer M, Mårtensson N and Freund H-J 1999 *Chem. Phys. Lett.* **310** 229
[22] Mullins D R 2001 *J. Electron Spectr. Relat. Phenom.* **114-116** 333
[23] Mullins D R, Kundakovic L and Overbury S H 2000 *J. Catal.* **195** 169
[24] Overbury S H, Mullins D R, Huntley D R and Kundakovic J 1999 *J. Catal.* **186** 296
[25] Moller P J, Li Z S, Egebjerg T, Sambi M and Granozzi G 1998 *Surf. Sci.* **402-404** 719
[26] Sambi M, Della Negra M, Granozzi G, Li Z S, Hoffmann Jorgensen J and Moller P J 1999 *Appl. Surface Sci.* **142** 146
[27] Price N J, Reitz J B, Madix R J and Solomon E I 1999 *J. Elect. Spectrosc. Relat. Phenom.* **98-99** 257
[28] Abbate M, Pen H, Czyzyk M T, de Groot F M F, Fuggle J C, Ma Y J, Chen C T, Sette F, Fujimori A, Ueda Y and Kosuge K 1993 *J. Electron Spectrosc. Relat. Phenom.* **62** 185
[29] Biener J, Bäumer M and Madix R J 1999 *Surf. Sci.* **432** 178
[30] Biener J, Bäumer M, Madix R J, Liu P, Nelson E J, Kendelewicz T and Brown Jr G E 1999 *Surf. Sci.* **441** 1
[31] Günther S, Esch F, Gregoratti L, Marsi M, Kisinova M, Schubert U A, Grotz P, Knözinger H, Taglauer E, Schütz E, Schaak A and Imbihl R 2000 *CP507, X-ray Microscopy: Proc. 6th Int. Conf.*ed W Meyer-Ilse (American Institute of Physics) p 219

[32] Günther S, Gregoratti L, Kiskinova M, Taglauer E, Grotz P, Schubert U A and Knözinger H 2000 *J. Chem. Phys.* **112** 5440
[33] Rodriguez J A 1996 *Surf. Sci. Rep.* **24** 223
[34] Beutler A, Strisland F, Sandell A, Jaworowski A J, Nyholm R, Wiklund M and Andersen J N 1998 *Surf. Sci.* **411** 111
[35] Jaworowski A J 2001 *PhD Thesis* Lund University, Sweden
[36] Leisenberger F P, Surnev S, Vitali L, Ramsey M G and Netzer F P 1999 *J. Vac. Sci. Technol.* A **17** 1743
[37] Surnev S, Vitali L, Ramsey M G, Netzer F P, Kresse G and Hafner J 2000 *Phys. Rev.* B **61** 13945
[38] Surnev S, Kresse G, Sock M, Ramsey M G and Netzer F P 2001 *Surf. Sci.* at press
[39] Surnev S, Kresse G, Ramsey M G and Netzer F P 2001 *Phys. Rev. Lett.* **87** 86102
[40] Leisenberger F P 1999 *PhD Thesis* University of Graz, Austria
[41] Leisenberger F P, Surnev S, Koller G, Ramsey M G and Netzer F P 2000 *Surf. Sci.* **444** 211
[42] Sock M, Surnev S, Ramsey M G and Netzer F P 2001 *Topics in Catal.* **14** 15
[43] Sawatzky G A and Post D 1979 *Phys. Rev.* B **20** 1546
[44] Colton R J, Guzman A M and Rabalais J W 1978 *J. Appl. Phys.* **49** 409
[45] Sambi M, Sangiovanni G, Granozzi G and Parmigiani F 1997 *Phys. Rev.* B **55** 7850
[46] de Groot F M F, Grioni M, Fuggle J C, Ghijsen J, Sawatzky G A and Petersen H 1989 *Phys. Rev.* B **40** 5715
[47] Chen J G, Kim C M, Frühberger B, De Vries B D and Touvelle M S 1994 *Surf. Sci.* **321** 145
[48] Antonsson H, Nilsson A, Martensson N, Panas I and Siegbahn P E M 1990 *J. Electron Spectrosc. Relat. Phenom.* **54-55** 601
[49] Andersen J N, Qvarford M, Nyholm R, Sorensen S L and Wigren C 1991 *Phys. Rev. Lett.* **67** 2811
[50] Henry C R 1998 *Surf. Sci. Rep.* **31** 231 and references cited therein
[51] Renaud G, Noblet M, Barbier A, Ulrich O, Revenant C, Borenstzein Y, Lazzari R, Jupille J and Henry C R 2001 *2nd International Workshop on Oxide Surfaces (IWOX 2) (Taos, NM, USA, 15–19 Jan. 2001)*
[52] Hävecker M, Knop-Gericke A, Schedel-Niedrig T and Schlögl R 1998 *Angew. Chem. Int. Ed. Engl.* **110** 2049
Hävecker M, Knop-Gericke A, Schedel-Niedrig T and Schlögl R 1998 *Angew. Chem. Int. Ed. Engl.* **37** 1939